REPORT DOCUMENTATION PAGE

Form Approved OMB NO. 0704-0188

1. REPORT DATE (DD-MM-YYYY)	2. REPORT TYPE	3. DATES COVERED (From - To)
14-05-2013	Final Report	1-May-2007 - 30-Sep-2008

4. TITLE AND SUBTITLE

Model Classes, Approximation, and Metrics for Dynamic Processing of Urban Terrain Data

5a. CONTRACT NUMBER
W911NF-07-1-0185

5b. GRANT NUMBER

5c. PROGRAM ELEMENT NUMBER
611103

6. AUTHORS

Richard Baraniuk, Ronald DeVore, Sanjeev Kulkarni, Andrew Kurdila, Stanley Osher, Guergana Petrova, Robert Sharpley, Richard Tsai, Hongkai Zhao

5d. PROJECT NUMBER

5e. TASK NUMBER

5f. WORK UNIT NUMBER

7. PERFORMING ORGANIZATION NAMES AND ADDRESSES

University of South Carolina Research Foundatio
901 Sumter ST, 5th floor Byrnes

Columbia, SC 29208 -0001

8. PERFORMING ORGANIZATION REPORT NUMBER

9. SPONSORING/MONITORING AGENCY NAME(S) AND ADDRESS(ES)

U.S. Army Research Office
P.O. Box 12211
Research Triangle Park, NC 27709-2211

10. SPONSOR/MONITOR'S ACRONYM(S)
ARO

11. SPONSOR/MONITOR'S REPORT NUMBER(S)
52559-MA-MUR.66

12. DISTRIBUTION AVAILIBILITY STATEMENT

Approved for Public Release; Distribution Unlimited

13. SUPPLEMENTARY NOTES

The views, opinions and/or findings contained in this report are those of the author(s) and should not contrued as an official Department of the Army position, policy or decision, unless so designated by other documentation.

14. ABSTRACT

Theory, algorithms, and software have been developed for the analysis and processing of point cloud sensor data for representation, analysis and visualization of complex urban terrain. These involve various parameterizations of terrain data based on implicit surface representations and adaptive multiscale methods that enable high resolution and enhance understanding of topology and geometric features. The wavelet and multi scale methods enable fast computation and allow for varying local resolution of the data depending on the local density of the point cloud.

15. SUBJECT TERMS

approximation theory, wavelets, multi resolution, implicit methods, level sets

16. SECURITY CLASSIFICATION OF:			17. LIMITATION OF ABSTRACT	15. NUMBER OF PAGES	19a. NAME OF RESPONSIBLE PERSON
a. REPORT	b. ABSTRACT	c. THIS PAGE			Andrew Kurdila
UU	UU	UU	UU		19b. TELEPHONE NUMBER: 540-231-8028

Report Title

Model Classes, Approximation, and Metrics for Dynamic Processing of Urban Terrain Data

ABSTRACT

Theory, algorithms, and software have been developed for the analysis and processing of point cloud sensor data for representation, analysis and visualization of complex urban terrain. These involve various parameterizations of terrain data based on implicit surface representations and adaptive multiscale methods that enable high resolution and enhance understanding of topology and geometric features. The wavelet and multi scale methods enable fast computation and allow for varying local resolution of the data depending on the local density of the point cloud. The implicit representations which are developed facilitate highly accurate approximation of signed distances to the sensed terrain surface. The level sets of the signed distance provide efficiently computed field of view from specified observation points. Collaboration among MURI focus groups has ylelded hybrid methods incorporating the best features of both approaches. Simulation and field experiments have been conducted to test the MURI methodologies. These include problems of sensor assimilation for autonomous navigation of urban terrain, surveillance, secure route planning, line of sight, target acquisition and a host of related problems.

Enter List of papers submitted or published that acknowledge ARO support from the start of the project to the date of this printing. List the papers, including journal references, in the following categories:

(a) Papers published in peer-reviewed journals (N/A for none)

Received		Paper
05/13/2013	22.00	Alexei Belochitski, Peter Binev, Ronald DeVore, Michael Fox-Rabinovitz, Vladimir Krasnopolsky, Philipp Lamby. Tree approximation of the long wave radiation parameterization in the NCAR CAM global climate model, Journal of Computational and Applied Mathematics, (07 2011): 0. doi: 10.1016/j.cam.2011.07.013
05/13/2013	47.00	Jian Liang, Hongkai Zhao. Solving Partial Differential Equations on Point Clouds, SIAM Journal on Scientific Computing, (01 2013): 0. doi:
05/13/2013	44.00	Jian Liang, Rongjie Lai, Tsz Wai Wong, Hongkai Zhao. Geometric Understanding of Point Clouds Using the Laplace Beltrami Operator, Proceedings of the CVPR, (08 2012): 214. doi:
05/13/2013	62.00	Qing Wang, Sanjeev R. Kulkarni, Sergio Verdu. Universal Estimation of Information Measures for Analog Sources, Foundations and Trends in Communications and Information Theory, (01 2009): 265. doi:
05/13/2013	63.00	Haipeng Zheng, Sanjeev R. Kulkarni, H. Vincent Poor. Attribute-Distributed Learning: Models, Limits, and Algorithms, IEEE TRANSACTIONS ON Signal Processing, (01 2011): 386. doi:
05/13/2013	61.00	Fernando Perez-Cruz, Sanjeev R. Kulkarni. Robust and Low Complexity Distributed Kernel Least Squares Learning in Sensor Networks, IEEE Signal Processing Letters, (04 2010): 355. doi:
05/13/2013	60.00	Qing Wang, Sanjeev R. Kulkarni, Sergio Verdu. Divergence Estimation for Multidimensional Densities Via k-Nearest =-Neighbor Distances, IEEE TRANSACTIONS ON Information Theory, (05 2009): 2392. doi:
05/13/2013	59.00	Aman Jain, Sanjeev R. Kulkarni, Sergio Verdu. Multicasting in Large Wireless Networks: Bounds on the Minimum Energy Per Bit, IEEE TRANSACTIONS ON Information Theory, (01 2011): 14. doi:
05/13/2013	58.00	Joel B. Predd, Sanjeev R. Kulkarni, H. Vincent Poor. A Collaborative Training Algorithm for Distribured Learning, IEEE TRANSACTIONS ON Information Theory, (04 2009): 1856. doi:
05/13/2013	57.00	Joel B. Predd, Robert Seiringer, Elliott H. Lieb, Daniel N. Osherson, H. Vincent Poor, Sanjeev R. Kulkarni. Probabalistic Coherence and Proper Scoring Rules, IEEE TRANSACTIONS ON Information Theory, (10 2009): 4786. doi:
05/13/2013	56.00	Chiu-Yen Kao, Richard Tsai. Properties of a Level Set Algorithm for the Visibility Problems, J Sci Comput, (03 2008): 170. doi:
05/13/2013	41.00	Ronald DeVore, Guergana Petrova, Matthew Hielsberg, Luke Owens, Billy Clack, Alok Sood. Processing Terrain Point Cloud Data, SIAM Journal on Imaging Sciences, (01 2013): 0. doi: 10.1137/110856009
05/13/2013	40.00	Abdellah Chkifa, Albert Cohen, Ronald DeVore, Christoph Schwab. Sparse adaptive Taylor approximation algorithms for parametric and stochastic elliptic PDEs, ESAIM: Mathematical Modelling and Numerical Analysis, (11 2012): 0. doi: 10.1051/m2an/2012027
05/13/2013	39.00	Albert Cohen, Ingrid Daubechies, Ronald DeVore, Gerard Kerkyacharian, Dominique Picard. Capturing Ridge Functions in High Dimensions from Point Queries, Constructive Approximation, (12 2011): 0. doi: 10.1007/s00365-011-9147-6
05/13/2013	38.00	J. Smith, G. Petrova, S. Schaefer. Encoding normal vectors using optimized spherical coordinates, Computers & Graphics, (08 2012): 0. doi: 10.1016/j.cag.2012.03.017

05/13/2013 37.00 ALBERT COHEN, RONALD DEVORE, CHRISTOPH SCHWAB. ANALYTIC REGULARITY AND POLYNOMIAL APPROXIMATION OF PARAMETRIC AND STOCHASTIC ELLIPTIC PDE'S, Analysis and Applications, (01 2011): 0. doi: 10.1142/S0219530511001728

05/13/2013 36.00 J. Manson, G. Petrova, S. Schaefer. Streaming Surface Reconstruction Using Wavelets, Computer Graphics Forum, (07 2008): 0. doi: 10.1111/j.1467-8659.2008.01281.x

05/13/2013 53.00 Ronald Devore, Guergana Petrova, Przemyslaw Wojtaszczyk . Instance-optimality in Probability with an l1-Minimization Decoder, Applied and Computational Harmonic Analysis, (05 2009): 275. doi:

05/13/2013 51.00 Hao Gao, Hengyong Yu, Stanley Osher, Ge Wang. Multi-Energy CT Based on a Prior Rank, Intensity and Sparsity Model (PRISM), Inverse Problems, (10 2011): 1. doi:

05/13/2013 50.00 Tom Goldstein, Xavier Bresson, Stanley Osher. Geometric Applications of the Split Bregman Method: Segmentation and Surface Reconstruction, J Sci Comput, (05 2009): 272. doi:

05/13/2013 55.00 Albert Cohen, Ronald DeVore, Ricardo H. Nochetto. Convergence Rates of AFEM with H-1 Data, Foundations of Computational Mathematics, (06 2012): 671. doi:

05/13/2013 27.00 Mark A Davenport, Chinmay Hegde, Marco F Duarte, Richard G Baraniuk. Joint Manifolds for Data Fusion, IEEE Transactions on Image Processing, (10 2010): 0. doi: 10.1109/TIP.2010.2052821

05/13/2013 26.00 J. Laska, Z. Wen, W. Yin, R. Baraniuk. Trust, but Verify: Fast and Accurate Signal Recovery from 1-bit Compressive Measurements, IEEE Transactions on Signal Processing, (2011): 0. doi: 10.1109/TSP.2011.2162324

05/13/2013 25.00 Chinmay Hegde, Richard G. Baraniuk. Sampling and Recovery of Pulse Streams, IEEE Transactions on Signal Processing, (04 2011): 0. doi: 10.1109/TSP.2010.2103067

05/14/2013 64.00 Albert Cohen, Wolfgang Dahmen, Ronald DeVore. Instance Optimal Decoding by Thresholding in Compressed Sensing, Contemporary Mathematics, (01 2010): 1. doi:

05/14/2013 65.00 Virginia Estellers, Dominique Zosso, Rongjie Lai, Stanley Osher, Jean-Philippe Thiran, Xavier Bresson. Efficient Algorithm for Level Set Method Preserving Distance Function, IEEE TRANSACTIONS ON Image Processing, (12 2012): 4722. doi:

08/30/2011 20.00 Peter Binev, Albert Cohen, Wolfgang Dahmen, Ronald DeVore, Guergana Petrova, Przemyslaw Wojtaszczyk. Convergence Rates for Greedy Algorithms in Reduced Basis Methods, SIAM Journal on Mathematical Analysis, (01 2011): 0. doi: 10.1137/100795772

08/30/2011 21.00 Peter Binev, Wolfgang Dahmen, Philipp Lamby. Fast high-dimensional approximation with sparse occupancy trees, Journal of Computational and Applied Mathematics, (02 2011): 0. doi: 10.1016/j.cam.2010.10.005

08/31/2011 23.00 M. Duarte, R. Baraniuk. Kronecker Compressive Sensing, IEEE Transactions on Image Processing, (08 2011): 0. doi: 10.1109/TIP.2011.2165289

08/31/2011 32.00 Sanjeev R. Kulkarni, H. Vincent Poor, Haipeng Zheng. Attribute-Distributed Learning: Models, Limits, and Algorithms, IEEE Transactions on Signal Processing, (01 2011): 0. doi: 10.1109/TSP.2010.2088393

08/31/2011 31.00 Ronald DeVore, Guergana Petrova, Przemyslaw Wojtaszczyk. Approximation of Functions of Few Variables in High Dimensions, Constructive Approximation, (6 2010): 0. doi: 10.1007/s00365-010-9105-8

08/31/2011 30.00 Sanjeev R. Kulkarni, Sergio Verdu, Aman Jain. Multicasting in Large Wireless Networks: Bounds on the Minimum Energy Per Bit, IEEE Transactions on Information Theory, (01 2011): 0. doi: 10.1109/TIT.2010.2090228

08/31/2011	29.00	Mark A. Davenport, Richard G. Baraniuk, Jason N. Laska, Petros T. Boufounos. Democracy in action: Quantization, saturation, and compressive sensing?, Applied and Computational Harmonic Analysis, (02 2011): 0. doi: 10.1016/j.acha.2011.02.002
12/20/2009	9.00	V. Cevher, A. Sankaranarayanan, M. F. Duarte, D. Reddy, R. G. Baraniuk, R. Chellappa. Compressive Sensing for Background Subtraction, Proceedings of the European Conference on Computer Vision (ECCV), (01 2008): . doi:
12/20/2009	13.00	M. A. Davenport, P. T. Boufounos, R. G. Baraniuk. Compressive domain interference cancellation, SPARSSignal Processing with Adaptive Sparse Structured Representations (2, (12 2009): . doi:
12/21/2009	15.00	V. Cevher, M. F. Duarte, R. G. Baraniuk. Distributed Target Localization via Spatial Sparsity, Proceedings of the European Conference on Computer Vision (ECCV), (01 2008): . doi:
12/21/2009	16.00	J.N. Laska, P.T. Boufounos, R.G. Baraniuk. Finite Range Scalar Quantization for Compressive Sensing, Proc. International Conference on Sampling Theory and Applications (SAMPTA), (12 2009): . doi:
12/21/2009	17.00	M.F. Duarte, C. Hegde, V. Cevher, R.G. Baraniuk. Recovery of Compressible Signals in Unions of Subspaces, Proceedings of the Conference on Information Sciences and Systems (CISS), (12 2009): . doi:
12/21/2009	18.00	V. Cevher, P. Indyk, C. Hegde, R.G. Baraniuk. Recovery of Clustered Sparse Signals from Compressive Measurements, Proc. International Conference on Sampling Theory and Applications (SAMPTA), (12 2009): . doi:
12/21/2009	19.00	V. Cevher, M. F. Duarte, C. Hegde, R.G. Baraniuk. Sparse Signal Recovery Using Markov Random Fields, Proceedings of the Workshop on Neural Information Processing Systems (NIPS), (12 2008): . doi:
TOTAL:	**40**	

Number of Papers published in peer-reviewed journals:

(b) Papers published in non-peer-reviewed journals (N/A for none)

Received		Paper
05/13/2013	49.00	Virginia Estellers, Dominique Zosso, Rongjie Lai, Stanley Osher, Jean-Philippe Thiran, Xavier Bresson. Efficient Algorithm for Level Set Method Preserving Distance Function, IEEE Transactions on Image Processing, (12 2012): 4722. doi:
TOTAL:	**1**	

Number of Papers published in non peer-reviewed journals:

(c) Presentations

5/2007-7/2008
R. Baraniuk, “Compressive Sensing: A New Framework for Computational Data Acquisition,” CAMSAP (Computational Advances in Multi-Sensor Adaptive Processing, St. Thomas, Virgin Islands, 2007.

R. Baraniuk, “Compressive Imaging for Vision Applications,” National Instruments Vision Summit, Austin, 2007.

R. Baraniuk, “Compressive Detection and Estimation via Smashed Filtering,” AMS 2007 von Neumann Symposium on Sparse Representation and High-Dimensional Geometry, 2007.

R. Baraniuk, “Compressive Imaging,” International Imaging Industry Association (I3A) 61st Annual Conference, Denver, 2007.

R. Tsai, IPAM Numerics and Dynamics for Optimal Transport, April 18, 2008.

R. Tsai, L1 Meeting at Texas A&M, May 17, 2008.

R. Tsai, AIMS Meeting at Arlington, TX, May 19, 2008.

R. Tsai, Workshop on Mathematical Imaging and Digital Media,
Singapore, June 18, 2008.

R. DeVore, Plenary talk 'Approximation and Learning in High Dimension,'
at Texas A&M University, College Station, TX, Oct 19-21, 2007;

R. DeVore and P.Binev,Plenary talks at the workshop 'Nonlinear
and Adaptive Approximations in High Dimensions' at Physikzentrum Bad
Honnef, Bonn, Germany, Dec 10-15, 2007;

P.Binev, Invited talk (Binev) at workshop 'Adaptive numerical methods for
PDE's' at Wolfgang Pauli Institute (WPI) Vienna, Austria, Jan 21-25,
2008;

P.Binev, Invited talk (Binev) at workshop 'Learning Theory and
Approximation' at MFO, Oberwolfach, Germany, June 29 - July 5, 2008;

H. Zhao, "Computing quasi-conformal maps between two arbitrary surfaces using discrete
Beltrami Flow" International Conference on Imaging Science, Hong Kong, 12/12-12/14, 2012.

8/2008 – 7/2009

R. Baraniuk, “Compressive Sensing Theory and Applications,” IMA (UK) Conference on Mathematics of Signal Processing VIII, Cirencester, UK, 2008.

R. Baraniuk, “Exploiting Sparsity through Compressive Sampling,” Workshop on Sparsity and its Application to Large Inverse Problems, Robinson College, Cambridge University, 2008.

R. Baraniuk, “Distributed Compressive Sensing,” Sensor, Signal, and Information Processing Workshop, Sedona, 2008.

R. Baraniuk, “An Introduction to Compressive Sensing,” DARPA IPTO Retreat, Annapolis, 2008.

R. Baraniuk, “Compressive Sensing, Wavelets, and Sparsity,” SPIE Defense + Security (acceptance speech for SPIE Wavelet Pioneer Award), Orlando, 2008.

R. Baraniuk, “Compressive Signal Processing,” 42nd Conference on Information Sciences and Systems (CISS), Princeton, 2008.

R. Baraniuk, “Compressive Signal Processing,” IAM-PIMS-MITACS Distinguished Colloquium Series, UBC, Vancouver, 2008.

Level Set Collective, April 7, 2009.

Southern California Nonlinear Control Conference at Caltech, May 22, 2009
National Taiwan University, Jul 10, 2009.

Workshop on Kinetic and Mean field models in the Socio-Economic Sciences, ICMS, UK, Jul 27, 2009.

Luke Owens, "Solving the Eikonal Equation on Adaptive Triangular and Tetrahedral Meshes", LSU, April 20th, 2009 .

Luke Owens, "Solving the Eikonal Equation on Adaptive Triangular and Tetrahedral Meshes", University of South Carolina, April 13 th, 2009 .

Robert Sharpley, "Dynamic Modeling of 3D Urban Terrain - a Multi-University Research Initiative", NATO SET-118, Columbia, SC, November 18, 2008.

Robert Sharpley, "Dynamic Modeling of 3D Urban Terrain with Accurate Topology and Geometry", NATO SET-118, Southampton, UK, April 27, 2009.

Peter Binev, "Adaptive Methods in Learning Theory", Peter Binev, seminar talk at University of Pittsburgh, Aug 21, 2009.

Peter Binev, "Learning Theory or how to extract knowledge from data," distinguishedlecture at University of Sofia, Bulgaria, Jul 13, 2009.

Peter Binev, "Coarsening in Adaptive Approximation", invited talk at 33rd SIAM-SEASConference, Columbia, SC, Apr 4, 2009.

Peter Binev, "Adaptive Methods and Near-Best Tree Approximation", seminar talk at University of Tel Aviv, Israel, Mar 12, 2009

B. Xu, D.J. Stilwell, and A.J. Kurdila, “Efficient Computation of Level Sets for Path Planning”, Proc. of IEEE/RSJ International Conf. on Intelligent Robots and Systems, Oct.11-15, 2009.

B. Xu, A.J. Kurdila, and D.J. Stilwell, “A Hybrid Receding Horizon Control Method for PathPlanning in Uncertain Environments”, Proc. of IEEE/RSJ International Conf. on Intelligent Robots and Systems, Oct. 11-15, 2009.

B . Xu, D. J. Stilwell, A. Gadre and A.J. Kurdila, “Analysis of local observability for featurelocalization in a maritime environment using an omnidirectional camera”, Proc. ofIEEE/RSJ International Conf. on Intelligent Robots and Systems, pp.3666-3671, Oct. 29-Nov.1, 2007.

Aug. 2009-Jul 2010

R. Baraniuk, “Randomized Dimensionality Reduction: A New Framework for Signal Processing and Communications,” IEEE International Symposium on Information Theory (ISIT), Seoul, Korea, 2009.

P. Binev, “On the Greedy Approach to Reduced Basis Method,” I Jaen Conference on Approximation, Ubeda, Jaen, Spain, July 4 - 9, 2010

P. Binev, “Nonlinear Approximation of Surfaces,” Seventh International Conference on Curves and Surfaces, Avignon, France, June 24 - 30, 2010

P. Binev, “Sparse Occupancy Trees, Workshop about High Dimensional Problems and Solutions,” Paris, France, June 21 - 22, 2010

P. Binev, “3D Reconstructions of Simulated Frequency Agile Lidar Sensed Concentration Fields,” 2010 DTRA/NSF Algorithm Workshop, Chapel Hill, NC, June 21-24, 2010.

P. Binev, “2.5 D Reconstructions of Simulated Frequency Agile LiDAR Concentration Estimates from a Fixed Location,” 2010 DTRA/NSF
Algorithm Workshop, Chapel Hill, NC, June 21-24, 2010.

P. Binev, “Adaptive Approximation of Surfaces,” International Conference on Constructive Theory of Functions, Sozopol, Bulgaria, June 3-9, 2010

P. Binev, “Adaptive Approximation of Surfaces,” Thirteenth International Conference in Approximation Theory, San Antonio, Texas, March, 6 - 10, 2010.

P. Binev, “Nonlinear Processing of HAADF STEM Data,” Imaging in Electron Microscopy II, Columbia, SC February 18 - 23, 2010.

R. Sharpley, “Segmentation and Compression of Heterogeneously Distributed 3D Point Clouds,” 3D Modelling of Urban Terrain - NATO SET 118, Ettlingen, Germany, November 3-5, 2009.

P. Binev, “Sparsity in Adaptive Approximation, Nonlinear and Adaptive Approximation,” Castle Reisensburg (Günzburg), Germany, September 30 -October 3, 2009.

Luke Owens, “An Algorithm for Surface Encoding and Reconstruction From 3D Point Cloud Data,” Numerical Analysis Seminar, Texas A&M, April 2010.

David Jimenez, “Matching of Point Configurations: An Approach Through Grammians,” Approximation Theory Conference, San Antonio, March 2010.

Guergana Petrova, “Instance-optimality in probability with an l1-minimization decoder,” Curves and Surfaces Conference, June, 2010.

R. Tsai, R. Takei, Y. Landa, and N. Tanushev, "A few optimal path planning problems and reversible cars with constrained turning radii", AFOSR Workshop on Computational Control, Nov 2009.

R. Tsai, Y. Landa, N. Tanushev, Y. Li, and S. Osher, "Inverse source problems in complicated domains," McGill University, Canada, Jan 2010.

R. Tsai and R. Takei, "Optimal trajectories for curvature constrained motions", Bar-Ilan University, Israel, May 2010.

R. Tsai, Y. Landa, N. Tanushev, Y. Li, and S. Osher, "Inverse source problems in domains with holes,” Technion University, Israel. June 2010.

R. Tsai, Y. Landa, N. Tanushev, Y. Li, and S. Osher, "Inverse source problems in domains with holes," NSF/DTRA Algorithm Workshop, June 2010.

8/2010-7/2011

P. Binev, "Localized Nonlocal Means with Application to Electron Microscopy"
Workshop on Wavelet and Multiscale Methods, Oberwolfach, Germany, August 1 - 7, 2010.

P. Binev, "High-Dimensional Scattered Data Approximation with Sparse Occupancy Trees", Workshop on Wavelet and Multiscale Methods, Oberwolfach, Germany, August 1 - 7, 2010.

P. Binev, "Greedy algorithms for the Reduced Basis Method", Multivariate Approximation and Interpolation with Applications, Edinburgh, UK
September 6 - 10, 2010.

R. Sharpley, "Mathematical methods for high resolution image formation from scanning transmission electron microscopy"
The Second International Conference on NUMERICAL ANALYSIS AND OPTIMIZATION, Muscat, OMAN, January 5, 2011.

P. Lamby, "Total Variation Regularization in Tomography- Part I"
New Frontiers in Imaging and Sensing Seminar Series, Columbia, SC
January 28, 2011.

P. Lamby, "Total Variation Regularization in Tomography- Part II"
New Frontiers in Imaging and Sensing Seminar Series, Columbia, SC
February 4, 2011.

D. Savu, "A Basic Concept in Compressive Sensing Applied to a STEM Image Reconstruction Problem" Workshop- New Frontiers in Imaging and Sensing, Columbia, SC, February 17 - 22, 2011.

P. Binev, "High Quality Image Formation by Unconventional Data Acquisition in STEM" Workshop- New Frontiers in Imaging and Sensing, Columbia, SC
February 17 - 22, 2011.

P. Lamby, "TV-Regularized Algebraic Reconstruction for Limited-Angle Tomography" Workshop- New Frontiers in Imaging and Sensing, Columbia, SC
February 17 - 22, 2011 B. Karaivanov, "Polygonal representation of 3D urban terrain point-cloud data- Part I" New Frontiers in Imaging and Sensing Seminar Series, Columbia, SC February 23, 2011.

B. Karaivanov, "Polygonal representation of 3D urban terrain point-cloud data- Part II" New Frontiers in Imaging and Sensing Seminar Series, Columbia, SC, March 3, 2011.

P. Binev, "Classification using nonlinear approximation," International Symposium on Approximation Theory, Nashville, TN, May 17 - 21, 2011.

P. Binev, "Point cloud processing using reliable sets," 2011 Algorithm Workshop, Boston, MA, June 7 - 9, 2011.

P. Binev, "Sparse Occupancy Trees for Approximation and Classification," Workshop on Theoretical Aspects of High-Dimensional Problems and Information- Based Complexity, Bonn, Germany, June 20 - 24, 2011
P. Binev, "Advanced Data Acquisition in Electron Microscopy," FoCM 2011 Workshop on Approximation Theory, Budapest, Hungary, July 8 - 10, 2011

P. Binev, "Advanced Image Formation in Electron Microscopy,"
Aachen Conference on Computational Engineering Science, Aachen, Germany
July 13 - 15, 2011

P. Binev, "Sparse Tree Approximation in High Dimensions," Applied Harmonic Analysis and Multiscale Computing, Edmonton, Canada, July 25 - 28, 2011.

H. Zhao, "Shape Reconstruction from Point Cloud," Dagstuhl-Seminar on "Innovations for Shape Analysis: Models and Algorithms"Schloss Dagstuhl - Leibniz- Zentrum fur Informatik, Germany.

April 2011, H. Zhao, "Analysis and Segmentation of Point Cloud",
International Workshop on Image Processing, Computer Vision, Compressive Sensing and Related Applications, Seoul, KOREA, December 2010.

R. DeVore, "Greedy Algorithms for High Dimensional Approximation,"
Foundations of Computa- tional Mathematics Conference, Budapest, Hungary,
July 4-14, 2011

R. DeVore, "Greedy Algorithms for Generating Reduced Bases,"
Aachen Conference on Computational Engineering Science, Aachen, Germany
July 13-15, 2011.

R. DeVore, "Approximation Theory," II Jaen Conference on Approximation Theory, Ubeda, Jaen, Spain, June 26 - July 1, 2011.

R. DeVore, "Reduced Basis," Reduced Basis Methods in High Dimensions Workshop, Paris, France, June 23-24, 2011.

8/2011-7/2012

R. Baraniuk, "Randomized Dimensionality Reduction and Compressive Sampling," Padovani Lecture, Information Theory School, IEEE Information Theory Society, Austin, 2011.

R. Baraniuk, “Compressive Sensing and Signal Processing,” University of Delaware Distinguished Lecture Series, 2011.

"On Adaptive Strategies in Finite Element Methods", Computational Methods in Applied Mathematics (CMAM2012) Berlin, Germany, July 30 - August 3, 2012.

"On the Greedy Approach to the Reduced Basis Method", Workshop on Model Order Reduction in PDE Constrained Optimization, Hamburg, Germany, July 25 - 27, 2012.

"Adaptive Partitioning Algorithms for Classification", Eighth International Conference on Mathematical Methods for Curves and Surfaces, Oslo, Norway, June 28 - July 3, 2012.

"Classification Algorithms using Adaptive Partitioning", Institute for Geometry and Practical Mathematics, RWTH - Aachen, Aachen, Germany, July 12, 2012.

"Greedy Approach to Reduced Basis Method", University of Hawaii, Honolulu, March 7, 2012.

“Manifold-based Signal Separation and Recovery,” International Workshop on Signal and Image Geometry Modelling and Approximation (SIGMA), Marseille, France.

“Open Education for Disaster Preparation,” FLASH 2012 Annual Conference, Orlando.

“Compressive Sensing: 8 Years After,” 46th Asilomar Conference on Signals, Systems, and Computers, Pacific Grove, CA

“Optimization based Sparse Signal Recovery,” 21st International Symposium on Mathematical Programming (ISMP 2012), Berlin

“Compressive Signal Processing,” Center for Advanced Signal and Image Science (CASIS) Workshop, Lawrence Livermore National Laboratory

“Compressive Signal Processing,” Mohammed Dahleh Distinguished Lecture, UCSB

"Greedy Algorithms in Banach Spaces", Paris, France, June 2012

"Lecture 1: Encoding Signals and Lecture 2: Image Compression", AICES Lectures, Aachen, Germnay, June 2012

"Greedy Algorithms in Banach Spaces", Davinci Lecture Series, Milan, Italy, July 2012

"Greedy Algorithms in Banach Spaces", Departmental Series, Aachen, Germany, July 2012

”Geometric Understanding of Point Clouds Using Laplace-Beltrami Operator”, Advances in Scientific Computing, Imaging Science and Optimization, in honor of Stanley Osher’s 70th birthday, IPAM, UCLA, 4/4-4/6, 2012.

”Solving partial differential equations on point clouds”, The International Confer- ence on Scientific Computing, in honor of Tony Chan’s 60th birthday, Hong Kong, 1/4-1/7, 2012.

H. Zhao, "Geometric Understanding of Point Clouds Using Laplace-Beltrami Opera-
tor", Advances in Scienti_c Computing, Imaging Science and Optimization,
IPAM, UCLA, 4/4-4/6, 2012.

H. Zhao, "Solving partial di_erential equations on point clouds", The International Conference on Scienti_c Computing, Hong Kong, 1/4-1/7, 2012.

H. Zhao, "Shape Reconstruction from Point Cloud", Dagstuhl-Seminar on "Innovations for Shape Analysis: Models and Algorithms", 4/2011, Schloss Dagstuhl - Leibniz-Zentrum fur Informatik, Germany.

H. Zhao, "Analysis and Segmentation of Point Cloud", International Workshop on Image Processing, Computer Vision, Compressive sensing and Related Applications, 12/2010, Seoul, Korea.

R. DeVore, Greedy Algorithms in Banach Spaces, Davinci Lecture Series, Milan, Italy, July 2012.

R. DeVore, Greedy Algorithms in Banach Spaces, Departmental Series, Aachen, Germany July 2012.

R. DeVore, Greedy Algorithms in Banach Spaces, Paris, France June 2012.

R. DeVore, Lecture 1: Encodingi Signals and Lecture 2: Image Compression, AICES Lectures, Aachen, Germany, June 2012.

D. Petrova, Sofia University, June 2012.

8/2012-1/2013
R. Baraniuk, “Video Compressive Sensing,” Matheon Workshop on Compressed Sensing and its Applications, Berlin, 2013.

R. Baraniuk, “Convex Optimization for Learning Near-Isometric Linear Embeddings,” GlobalSIP 2013 Symposium on Low-Dimensional Models and Optimization in Signal Processing, Austin, TX, 2013

R. Baraniuk, “Sparsity and Signal Processing,” SPARS Workshop, EPFL, Lausanne, Switzerland
“Video Compressive Sensing,” BASP Frontiers Workshop, Switzerland, 2013.

Number of Presentations: 107.00

Non Peer-Reviewed Conference Proceeding publications (other than abstracts):

Received Paper

TOTAL:

Number of Non Peer-Reviewed Conference Proceeding publications (other than abstracts):

Peer-Reviewed Conference Proceeding publications (other than abstracts):

Received	Paper	
05/13/2013	24.00	J. P. Slavinsky, Jason N. Laska, Mark A. Davenport, Richard G. Baraniuk. The compressive multiplexer for multi-channel compressive sensing, ICASSP 2011 - 2011 IEEE International Conference on Acoustics, Speech and Signal Processing (ICASSP). 2011/05/22 00:00:00, Prague, Czech Republic. : ,
08/31/2011	33.00	Sang-Mook Lee, Jeong Joon Im, Bo-Hee Lee, Alexander Leonessa, Andrew Kurdila. A real-time grid map generation and object classification for ground-based 3D LIDAR data using image analysis techniques, 2010 17th IEEE International Conference on Image Processing (ICIP 2010). 2010/09/26 00:00:00, Hong Kong, Hong Kong. : ,
08/31/2011	34.00	Bin Xu, Daniel J Stilwell, Andrew J Kurdila. A receding horizon controller for motion planning in the presence of moving obstacles, 2010 IEEE International Conference on Robotics and Automation (ICRA 2010). 2010/05/03 00:00:00, Anchorage, AK. : ,
TOTAL:	**3**	

Number of Peer-Reviewed Conference Proceeding publications (other than abstracts):

(d) Manuscripts

Received	Paper	
05/13/2013	48.00	Jian Liang, Frederick Park, Hongkai Zhao. Robust and Efficient Implicit Surface Reconstruction for Point Clouds Based on Convexified Image Segmentation, J Sci Comput (03 2012)
05/13/2013	46.00	Rongjie Lai, Jiang Liang, Hongkai Zhao. A Local Mesh Method for Solving PDES on Point Clouds, Inverse Problems and Imaging (01 2012)
05/13/2013	43.00	Songting Luo, Leonidas Guibas, Hong-Kai Zhao. Euclidean skeletons using closest points, Inverse Problems and Imaging (02 2011)
09/23/2008	1.00	. Anisotropic Smoothness Spaces via Level Sets, ( )
09/23/2008	2.00	Yanina Landa, Richard Tsai. Visibility of Point Clouds and Exploratory Path Planning in Unknown Environments, ( )
11/30/2009	3.00	Yanina Landa, Haochong Shen, Ryo Takei, and Yen-Hsi R. Tsai. Autonomous Source Discovery and Navigation in Complicated Environments, IEEE International Conference on Robotics and Automation (11 2009)
11/30/2009	5.00	Martin Burger, Yanina Landa, Nicolay M. Tanushev, Richard Tsai. Discovering a Point Source in Unknown Environments, Eighth International Workshop on the Algorithmic Foundations of Robotics (01 2008)
11/30/2009	6.00	Ryo Takei, Richard Tsai, Haochong Shen, Yanina Landa. A Practical Path-planning Algorithm for a Vehicle with a Constrained Turning Radius: a Hamilton-Jacobi Approach, Automatic Control (11 2009)
12/01/2009	7.00	E. Castillo, H. Zhao. Point Cloud Segmentation via Constrained Nonlinear Least Squares Surface Normal Estimates, Twenty-Third IEEE Computer Society Conference on Computer Vision and Pattern Recognition (12 2009)
12/01/2009	8.00	Y. Xi, Y. Duana, H. Zhao. A Nonparametric Approach for Noisy Point Data Preprocessing, International Journal of CAD/CAM (12 2009)
12/20/2009	10.00	J. N. Laska, P. T. Boufounos, M. A. Davenport, R. G. Baraniuk. Democracy in Action: Quantization, Saturation, and Compressive Sensing, IEEE Transactions on Signal Processing (12 2009)
12/20/2009	11.00	R. G. Baraniuk, V. Cevher, M. F. Duarte, C. Hegde. Model-Based Compressive Sensing, IEEE Transactions in Information Theory (12 2009)
12/20/2009	12.00	C. Hegde, M F. Duarte, V. Cevher. Compressive Sensing Recovery of Spike Trains Using A Structured Sparsity Model, Proc. Workshop on Signal Processing with Adaptive Sparse Representations (SPARS) (12 2009)
TOTAL:	**13**	

Number of Manuscripts:

Books

Received	Paper

TOTAL:

Patents Submitted

Patents Awarded

Awards

Richard Baraniuk, SPIE Compressive Sampling Pioneer Award, 2012.
Richard Baraniuk, IEEE Signal Processing Educator Award, 2010.
Ronald DeVore, Gold Medal of the French Mathematical Society, 2011.
Stanley Osher, Fellow of the Society of Industrial and Appied Mathematics, 2009.
Stanley Osher, Elected to the American Academy of Arts and Sciences, 2009.
Stanley Osher, Honorary Doctoral Degree, Hong Kong Baptict University, 2009.
Stanley Osher, Plenary Speaker, International Conference of Mathematicians, 2010.
Stanley Osher, John von Neumann Lecture for the 2013 SIAM Annual Meeting, 2013.
Stanley Osher, Fellow of the American Mathematical Society, 2012.

Graduate Students

NAME	PERCENT SUPPORTED	Discipline
Aditya Kumar	0.04	
Alexander Mamonov	0.14	
Ali Ayremlou	0.04	
Ali Haddad	0.09	
Ali Mousavi	0.04	
Alok Sood	0.03	
Aman Jain	0.09	
Andrew Temylakov	0.08	
Andrew Waters	0.03	
Ben Smith	0.10	
Billy Clack	0.05	
Bin Dong	0.15	
Bin Xu	0.10	
Chinmay Hegde	0.03	
Daniel Calderon	0.04	
Daniel Savu	0.04	
Daniel Soares	0.02	
Dharmpal Takhar	0.02	
Edward Castillo	0.13	
Francisco Blanco-Silva	0.09	
Gil Ariel	0.12	
Guanchun Wang	0.26	
Haipeng Zheng	0.12	
Haochong Shen	0.03	
Huiyi Hui	0.06	
Igor Yanovsky	0.11	
Jason Laska	0.05	
Jeong Im	0.00	
Jian Liang	0.25	
Jieqi Yu	0.27	
John Freeman	0.02	
Kamala Diefenthaler	0.02	
Manjari Narayan	0.10	
Marco Duarte	0.01	
Mark Davenport	0.02	
Matthew Moravec	0.05	
Matthew Summers	0.09	
Michael Bennet	0.22	
Mona Sheikh	0.09	
Moritz Allmaras	0.06	
Nicolay Tanushev	0.14	
Petros Boufounos	0.05	
Philipp Lamby	0.11	
Seong Jun Kim	0.04	
Shang Shang	0.03	
Shriram Sarvotham	0.03	
Teng Wang	0.04	
Ting Sun	0.04	
Volkan Cevher	0.03	
Woon Kim	0.10	
Xinwei Zhang	0.11	
Yingying Li	0.02	
Yu Lei	0.14	
Yue Li	0.02	
Zhuo Zhang	0.09	
FTE Equivalent:	**4.29**	
Total Number:	**55**	

Names of Post Doctorates

NAME	PERCENT_SUPPORTED
Alexander Mamonov	0.28
Aswin Sankaranarayanan	0.10
Colin Macdonald	0.01
Edward Castillo	0.44
Frederic Park	0.58
Gil Ariel	0.12
Nicolay Tanushev	0.14
Vahram Stepanyan	0.01
Yanina Landa	0.38
FTE Equivalent:	**2.06**
Total Number:	**9**

Names of Faculty Supported

NAME	PERCENT_SUPPORTED	National Academy Member
Andrew Kurdila	0.09	
Guergana Petrova	0.17	
Hongkai Zhao	0.08	
Mark Pierson	0.03	
Michael Roan	0.02	No
Peter Binev	0.09	
Richard Baraniuk	0.00	
Richard Tsai	0.19	
Robert Sharpley	0.11	
Ronald DeVore	0.03	
Sanjeev Kulkarni	0.08	
Stanley Osher	0.13	Yes
Wolfgang Dahmen	0.02	
FTE Equivalent:	**1.04**	
Total Number:	**13**	

Names of Under Graduate students supported

NAME	PERCENT_SUPPORTED	Discipline
Josiah Manson	0.11	computer science
Peter Hall	0.05	mathematics
Matthew Madison	0.04	mathematics
Randy Ransom	0.11	computer science
Miquel Borromeo	0.01	computer science
Elizabeth Timko	0.01	mathematics
Ryan Tanghe	0.01	mathematics
Alok Sood	0.03	computer science
Billy Clack	0.05	computer science
Casey Rodriguez	0.09	computer science
Charles Arnold	0.05	mathematics
Deepanshu Arora	0.02	mechanical engineering
FTE Equivalent:	**0.58**	
Total Number:	**12**	

Student Metrics

This section only applies to graduating undergraduates supported by this agreement in this reporting period

The number of undergraduates funded by this agreement who graduated during this period:	12.00
The number of undergraduates funded by this agreement who graduated during this period with a degree in science, mathematics, engineering, or technology fields:.....	12.00
The number of undergraduates funded by your agreement who graduated during this period and will continue to pursue a graduate or Ph.D. degree in science, mathematics, engineering, or technology fields:.....	7.00
Number of graduating undergraduates who achieved a 3.5 GPA to 4.0 (4.0 max scale):	3.00
Number of graduating undergraduates funded by a DoD funded Center of Excellence grant for Education, Research and Engineering:	0.00
The number of undergraduates funded by your agreement who graduated during this period and intend to work for the Department of Defense	0.00
The number of undergraduates funded by your agreement who graduated during this period and will receive scholarships or fellowships for further studies in science, mathematics, engineering or technology fields:	3.00

Names of Personnel receiving masters degrees

NAME	
Matthew Moravec	
Manjari Narayan	
Yu Lei	
Dante Soares	
Haochong Shen	
Benjamin Ingram	
Alok Sood	
Aditya Kumar	
Total Number:	**8**

Names of personnel receiving PHDs

NAME	
Bin Dong	
Huiyi Hui	
Yingying Li	
Haochong Shen	
Teng Wang	
Jieqi Yu	
Aman Jain	
Haipeng Zheng	
Guanchun Wang	
Jiang Liang	
Seong Jun Kim	
Woon Kim	
Yu Lei	
Bin Xu	
Mark Davenport	
Marco Duarte	
Chinmay Hegde	
Jason Laska	
Shriram Sarvotham	
Mona Sheikh	
Ting Sun	
Darmpal Takhar	
New Entry	
Moritz Allmaras	
Total Number:	**24**

Names of other research staff

NAME	PERCENT_SUPPORTED
Matt Hielsberg	0.16
Jonathan Winters	0.15
Emil Dotchevski	0.27
Janice Long	0.22
J.P. Slavinsky	0.10
Justin Farmer	0.02
FTE Equivalent:	**0.92**
Total Number:	**6**

Sub Contractors (DD882)

Inventions (DD882)

5 **Polyphase Random Demodulation**

Patent Filed in US? (5d-1) Y

Patent Filed in Foreign Countries? (5d-2) N

Was the assignment forwarded to the contracting officer? (5e) N

Foreign Countries of application (5g-2):

5a: Richard Baraniuk

5f-1a: Rice University

5f-c: 6100 Main Street

Houston TX 77005

Scientific Progress

See Attachment

Technology Transfer

FIFTH ANNUAL REPORT: ARO MURI
AWARD # W911NF-07-1-0185

SUBMITTED BY ANDREW KURDILA, PI

On Behalf of Institutional PI's
Richard Baraniuk (Rice), Sanjeev Kulkani (Princeton),
Stanley Osher (UCLA), Guergana Petrova (TAMU), Ronald DeVore & Robert Sharpley (USC)
Richard Tsai (Texas), Hongkai Zhao (UC Irvine)

OVERVIEW

This report summarizes efforts and accomplishments of the eight universities collaborating on Multi-University Research Initiative of the Army Research Office (ARO), grant W911NF-07-1-0185, entitled *Model Classes, Approximation, and Metrics for Dynamic Processing of Urban Terrain Data.* This project has developed theory, algorithms, software and experiments for the synthesis of urban terrain maps from dynamic point cloud sensor data.

The main goals of the research team have been (i) to capture high order topology through implicit representation of surfaces, (ii) to develop multiscale and adaptive algorithms which enable various resolutions of the rendered surface governed by the local density of the point clouds, (iii) to derive algorithms for fast computation of signed distances to the terrain surface thereby giving field of view from specified observation points, (iv) to derive fast and efficient methodologies for the use of dynamic point cloud measurements for the navigation and control of autonomous vehicles in three dimensions, and (v) to develop change detection theory and methods that employ point cloud observations taken at different times.

CONTENTS

1. COMPRESSION OF POINT CLOUDS

Terrain point cloud data are typically acquired through some form of LiDAR sensing or from post-processing CCD image sequences via feature point tracking algorithms. They form a rich resource that is important in a variety of applications including navigation, line of sight calculations, and terrain visualization. The point clouds themselves are too cumbersome and large to be used directly for these purposes. They need to be converted to a simpler platform that is more efficient and still contains all of the features of the terrain, present in the point cloud, that are needed for these applications. A naive approach would be to take local averages of data heights to obtain pixel intensities (and therefore a pixelized image) and then employ the techniques of image processing to make a conversion into a wavelet or other multiscale representation. However, this approach is not successful for several reasons. Foremost among these is that terrains are not images. They have certain topology and geometry that must be extracted and preserved. A second related point is that the usual least squares metrics used in image processing do not match the intended applications for terrain maps. For example, capturing long thin structures such as poles, towers, and wires are essential for navigation, but are not given priority in PSNR metrics employed for images. Another issue is that terrain point clouds usually have missing data, occlusions and noise which do not appear in many other applications. While surface reconstruction from point clouds is now a dominant theme in computer graphics, very little of this work addresses terrain data per se. Of course, one could argue that one can simply apply one of the vast number of surface processing algorithms in computer graphics. However, these algorithms are typically built for high resolution data which is not the case for general terrain data, which suffers from occlusions, missing data, noise, and variable resolution.

Our platform for urban/terrain processing is built on the following principles:

- Distortion is measured in the Hausdorff metric, which we argue is a good match for the application demands.
- The decomposition is organized in a multiscale octree giving coarse to fine resolution.
- Each node of the tree corresponds to a dyadic cube and is equipped with a low degree polynomial fit to the point cloud on this cube that minimizes the local Hausdorff error of this fit.
- The tree is organized into subtrees each of which corresponds to a certain accuracy of resolution in the Hausdorff metric.
- The tree and nodal information can be efficiently encoded using predictive encoding.
- Upon receiving the tree and nodal information, the user can easily convert this information to a format that matches the intended application.
- Primitives such as normals, curvature, and other information can be extracted from the tree and nodal information.

This may be the only terrain point cloud encoder that gives rate/distortion performance and the only encoder using the Hausdorff metric. There are no other studies known to us with which we could compare our work. This lack of documented encoding algorithms has been one of the drawbacks in the development of terrain point cloud encoding. The MURI encoder, as described in [26], gives a benchmark to which other researchers can now compare their work.

1.1. **Targeted Applications Guiding Algorithm Development.**

To demonstrate the applicability of the techniques being developed in this project, we have focused on several targeted applications that we now describe.

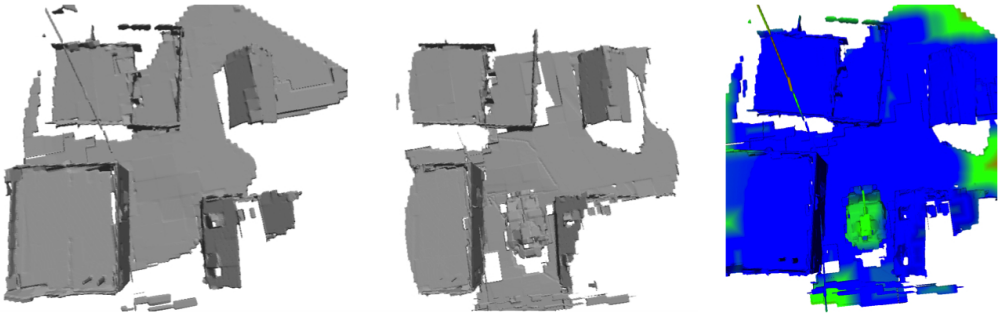

FIGURE 1. Two reconstructions (left and middle) from point cloud scans generated from separate flyovers of a simulated aerial vehicle. The combined surface (right) is colored according to the distance between the surfaces. Blue indicates little to no difference while green and red indicate larger differences in the surfaces.

Change Detection: We have consulted with ARL researchers at Adelphi and AFRL sensors directorate personnel at Wright Patterson to formulate a problem which illustrates the potential of the algorithms, while addressing the RCAs of the MURI effort. A timely and relevant problem which satisfies these criteria is the problem of change detection in geometric scenes imaged by fixed and mobile surveillance platforms equipped with various sensor packages. Given two sets of point cloud data of a given scene, generated at different times, we would like to identify any changes that have taken place in the scene. The ultimate goal of this application is to have algorithms which can be applied to point cloud data generated in real time by a battery of navigating sensors.

We have incorporated our encoder, together with various denoising and enhancement routines in order to demonstrate a proof of concept. We have developed simulated LIDAR point clouds of scenes which share some common regions, incorporated changes in these scenes and have run our algorithms on each scene to see if it can identify the changes. To compute changes, we measure the Hausdorff distance between the two reconstructed surfaces we generate. Figure 1 shows the performance of our algorithm on a typical example where the one point cloud is of a scene with a tank sitting in an alley between two buildings.

Path Planning: Next, we have collaborated with researchers from UT and USC and performed several experiments using the USC Simulator, TAMU Surface Reconstruction methods and UT path planning algorithms to fully navigate autonomous vehicles. In our tests, a simulated LiDAR device was positioned and a scan of the environment performed. The resulting scan data was used to reconstruct the visible surfaces. From the approximated surface and sensor location a visibility volume was produced and processed by the UT path planner in order to move the sensor to its next position, see Figure 2.

Low Power Communication: We acknowledge that many defense missions require real-time visualization of reconstructed surfaces on low power bandwidth-limited devices. Our encoding scheme allows for such devices to receive encoded surfaces in a progressive streaming fashion. The TAMU group has developed and demonstrated that these encoded surfaces can be decoded and reconstructed for visualization on current consumer tablet and smart phone technology, see Figure 3.

LIDAR Simulation: One of the difficulties in testing any algorithm is the availability of suitable data. Acquisition of real data can not only be time consuming but may also be too costly and

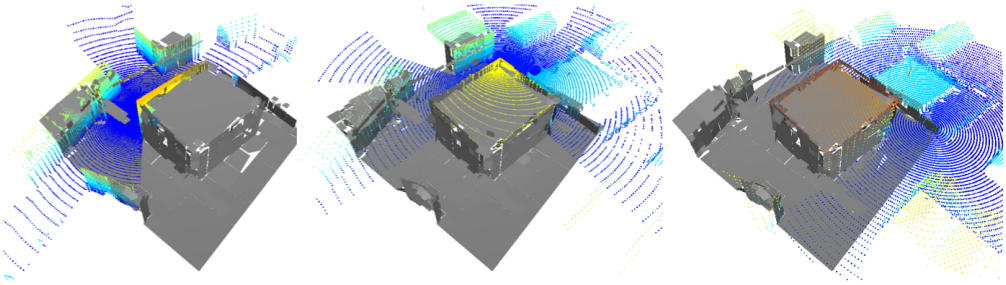

FIGURE 2. An example set of three aggregate reconstructions from a closed-loop simulation using the UT path planner and TAMU Surface Reconstruction. Each reconstruction shows a single scan, colored by height, that was used to update the reconstruction.

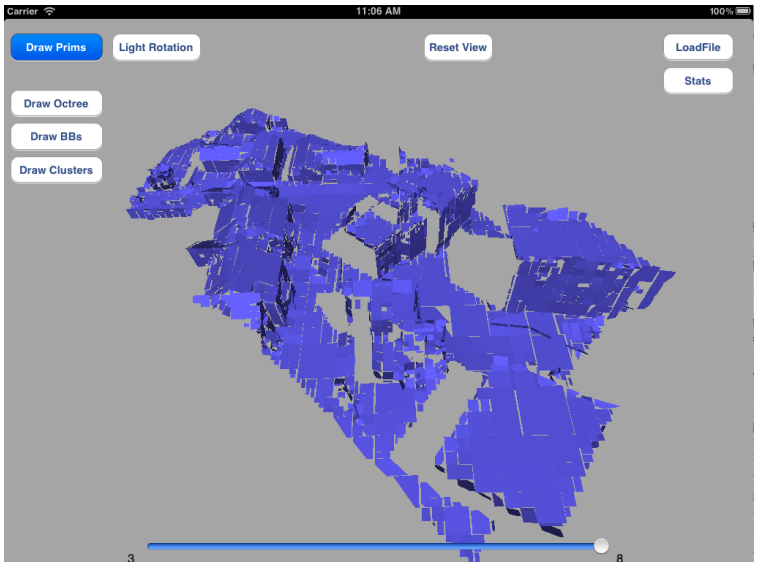

FIGURE 3. A snapshot of the TAMU Surface Viewer running on an iPad. The surface shown has been decoded and reconstructed locally on the iPad for display.

perhaps impossible with available sensors and vehicles. To address this, as a part of our outreach program, we have developed an editor for 3D point clouds that can work with data produced by the USC Simulator in order to construct point clouds suitable for testing. The point cloud editor supports basic operations such as cut, trim, copy and paste along with more advanced operations including denoising. The editor is publicly available as part of the latest PCL (pointclouds.org) source release. In addition, Matthew Hielsberg, a researcher at TAMU, has coordinated with PCL staff and the PCL community to identify a set of existing repositories for both point cloud data and point cloud processing packages. As a result of this collaboration the PCL website will now house a permanent set of up-to-date links for the community (http://pointclouds.org/media/), see Figure 4.

1.2. **Algorithm Development.** Next, we will describe in some details our algorithms. The encoder assigns bits to determine the occupancy tree, and to determine each of the polynomials on the terminal leaves. The result is a compression of the original point cloud into a succinct progressive bitstream. Typical compression rates are from 100-1 up to 500-1 depending on the complexity

FIGURE 4. A snapshot of the prototype site put together for the PCL community. This site is to serve as a central location for the storage of links to publicly available data and software for the processing of point cloud and related data.

of the point cloud. At these compression rates, the essential geometry and topology of the underlying terrain surface are preserved and high quality reconstruction is possible from the compressed file, see [26]. We have collaborated with USC in the generation of the occupancy tree and with Rice by employing their predictive tree encoding algorithms to enhance the compression rates. An alternative to the Rice encoder was proposed in [50], where a compression of the octree structure together with the linear functions at each of its nodes is presented. The encoding of a linear function at a node is performed by encoding the distances from three points associated with that node to the linear function and an additional bit. The reconstruction is done by solving a simple linear optimization problem with a nonlinear constraint.

During the grant period, several essential difficulties have been resolved in the encoding and display algorithms. In the encoding, it has been noted that to achieve the required Hausdorff error, several refinements are made because the distance from the compressed surface to the point cloud is large due to the fact that the compressed surface on a given cube often extends far away from the point cloud. To resolve this difficulty and improve encoding the idea of bounding boxes has been introduced and analyzed. Although bounding boxes add some overhead to encoding, this overhead is more than compensated for by reducing the size of the final tree.

When receiving the compressed file, the receiver needs an algorithm for surface reconstruction and display from the encoded bitstream. This is perhaps the most significant challenge in terrain encoding. The main obstacle is the identification of the inside and outside of the surface from the local polynomial fits. In other application domains of surface compression, this is accomplished by determining normals to the surface. These are either assumed to be given by the sensor or else are computed using the high resolution of the point cloud. Neither of these alternatives are available with standard terrain point clouds. This problem has been resolved during the grant period by determining which side of the plane is in the interior of the surface using sophisticated labeling and marching algorithms. These algorithms are challenged by the occlusions and missing data.

Our algorithm resolves this by assigning cubes of high altitude as out and those of low altitude as in. Both of these types of cubes typically have no data in them. Then a marching strategy makes an assignment of inside and outside on all of the occupied cubes. This is done so that there is a self consistency. The portions of the cube are then unioned to obtain a solid region in 3D whose boundary is the surface. Thus the surface is the level set having an implicit representation of the solid region. This implicit representation is important because it allows one to treat features such as overhangs and wires which functional representations would not allow.

The main advantage of using an implicit representation is its flexibility and robustness in dealing with complicated topology and automatic representation of holes or gaps after surface reconstruction. Implicit representation also allows one to generate distance fields which are useful for estimation of the Hausdorff metric, autonomous navigation, line of sight calculations and other operations. The above implicit representation is typically not smooth. However, our decoder allows the receiver to reconstruct smoother surfaces using the technology of Mason-Petrova-Schaefer [44] using implicit wavelet fits.

Octree Representation Under the Hausdorff Distance: We previously proposed a framework for representing a point cloud with a parametric union of piecewise polynomial surfaces that locally capture the geometry of the point cloud at various scales and translations. This representation is encoded in an octree data structure, where children nodes encode the information in a region at a finer level of detail than what is captured at the parent node. While octree representation has been well studied in the literature, our main innovation was the explicit use of the Hausdorff distance to control the fidelity of our representation.

The Hausdorff distance measures the "worst-case" deviation between the point cloud and surface. In contrast, the standard least-squares or L^2 metric measures only average deviation. While the L^2 metric is standard in literature, it performs rather poorly when representing thin structures such as light poles or telephone wires that have a small number of points. Poor representation of these thin structures can have a negligible impact under the L^2 distance, but is easily detected under the Hausdorff distance. While our initial strategy used the Hausdorff distance to measure the fidelity between the point cloud and the surface representation, the underlying fits that we chose were still L^2-optimal fits. The reason for this was simplicity; least-squares fitting is well understood, easy to implement, and computationally efficient. By contrast, Hausdorff optimal fitting is known to be NP hard. While our previous representation scheme is functional, there is often a significant gap between the Hausdorff-optimal and L^2-optimal fit. This had the practical effect of requiring an excessive number of nodes to represent the underlying data.

During the grant period, we have made significant progress in closing this performance gap. In particular, we have devised methods for creating fits that are optimal in the d_1 side of the Hausdorff metric, optimizing the distance measured from the point cloud to the surface. The one-sided Hausdorff distance from the points to the plane can be accomplished easily via projection and taking the maximum. Since the one-sided Hausdorff distance only depends on the distance from the points to the surface, it can be computed with simple projection operations and taking the maximum. Because of this, we can quickly search an allowable dictionary of fits to find the d_1-optimal fit. Additionally, we have shown that d_1-optimal planar fits actually provide a tight bound to the two-sided Hausdorff distance, D_H. This bound is dependent only on the magnitude of the one-sided Hausdorff distance and the size of the interpoint spacing of the data. The interpoint spacing can be solved with what is known as the largest empty circle problem [47] which can be solved in $O(N \log N)$ time, where N is the number of points under consideration. This need only be solved

once per node, and adds little computational overhead to our method. This bound not only establishes the worst-case value of D_H for our fit, but also the worst case D_H for any planar fit available in our surface dictionary.

At the heart of our encoding scheme is the issue of quantization. We wish to sufficiently truncate the cost to represent a surface while still preserving its fidelity. We wish to avoid using an excessive bitrate for encoding while simultaneously providing sufficient resolution. A known result for the L^2 error metric is that one must double the resolution of coefficients as one moves from high order to low order terms [21] to achieve optimal encoding. This result, as one might expect, does not hold under the Hausdorff metric for the case of planar fits. In particular we have shown that the Hausdorff error incurred through quantization of the constant term is identical to the quantization in the linear term. This allows us to use fewer bits in the constant term while maintaining the same Hausdorff fidelity, which reduces our overall encoding rate significantly.

We demonstrated the performance of our encoder on a simple data set involving a LiDAR scan of a house. We compare against the well known surflets method of Chandrasekaran [21], which is known to be optimal in the L^2 metric. However, because their method employs the L^2-distance it has difficulty detecting features such as the window on the house and does not sufficiently prune in the surface fits near the roof until the tree has been refined to an extremely deep level.

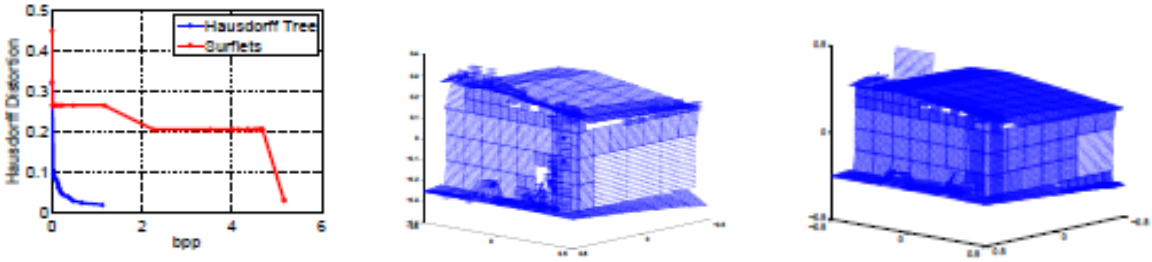

(a) (b) (c)

FIGURE 5. Left: Comparison between our method (Hausdorff Tree) with the L^2 Optimal Method of Chandrasekaran, et al. Our method achieves superior Hausdorff error with far fewer bits in the final encoding. Center: Hausdorff tree reconstruction at 1 bits/point. Right: The surflets reconstruction at 1 bits/point fails to capture the window of the house and does not adequately prune the roof.

2. LEARNING-RELATED ALGORITHMS

The elements of Mathematical Learning theory and its variants are particularly relevant to synthesis and analysis of urban terrain data in several respects. USC, Virginia Tech, and TAMU have a long ongoing project to develop novel methods to optimally learn surfaces from point cloud data. For example, this group has developed new theory and algorithms for sparse occupancy trees [9], classification from sets [5], and their application to processing point cloud data [3].

As described in Section 1.2, the implicit use of its principles leads to algorithm designs for synthesis, based upon local statistics and metrics, which adaptively partition point cloud space in order to construct multi-level approximate surfaces of objects imaged by sensors.

In Subsection 2.1, we describe work done during the current period on learning surfaces from point clouds where metadata is available on sensor position and pose. In this case, reconstruction

ambiguities can be resolved and more detailed topological properties can be determined in sensor parameter space. See Subsection 2.1 and its application in Section 5. This can also be integrated with registration of geometric features between different scans in a SLAM setting in order to estimate sensor pose and position.

Another learning-related problem involves properly aligning multiple data scans of a targeted region of urban terrain with the objective of either enhanced imaging, or for change detection. The data may be collected at different times from possibly different physical sensor states or by using sensors situated at multiple locations. For proper aggregation of the data, however, reliable, highly accurate registration of the collections is necessary, otherwise improper registration will result in a significant blurring of the reconstruction versus that which is produced by each of the collections individually. As reflected in the Eglin push-broom lidar collection, which we use extensively for testing, multiple passes cannot be aligned using rigid motion registered adjustments alone. This is due to distortions produced by noise in estimating the moving sensor platform's position and pose, but also significantly by the fact that the sensor is performing line scans as the platform is turning, with velocity components along the direction of the turn. If the sensor line scans are left to right, then right turns result in elongation in the scan while left turns lead to a dilation. In the perceived data, this has the effect of localized nonlinear distortions (stretching/shrinking) of an imaged surface. In Subsection 2.2 a nonlinear multi-level point cloud registration method is proposed, which is a completely analogous extension of our 2D work on time series scans used in microscopy imaging [4]. The basic localized registration procedure is described and applied to multiple airborne lidar swaths to demonstrate the algorithm's potential.

Nonlinear registration involves iteration and is substantially accelerated by identifying a set of local features within the point cloud which may be used as high quality markers for the the 6 degree of freedom local alignment. Methods for extracting structure and features from point cloud data are reported in Subsection 2.3 and Subsection 4.2, as reported in [33] and [16], respectively. Further as the data sets are more accurately aligned and the point cloud data unioned, more accurate reconstructions of the feature points themselves may be obtained, and used to further improve the registration process applied to the original raw point clouds.

Subsection 2.4 describes joint work between USC and TAMU personnel on extracting embedded information from data along with quantifiable estimates of the probability and risk associated with classification of the information. The algorithms developed in this MURI are robust with respect to the ambient dimension. For example, sparse occupancy trees allows processing algorithms whose complexity is proportional to the size of the data set rather than the ambient space dimension thereby defeating the curse of dimensionality in high dimensional settings. This is important because in many real world applications of point cloud data, for example hyper spectral data, can be viewed as high dimensional problems. Traditional numerical algorithms suffer from the curse of dimensionality which make them useless if the ambient dimension is even moderately high (larger than 10 for example). The collaboration between USC, VT, and TAMU injects new models for high dimensional functions based on sparsity and variable reduction which allows processing high dimensional data. For example, new theory and algorithms have been developed for classification in [5] by exploiting occupancy trees and new models for high dimensional functions. These algorithms have provable high order convergence under margin conditions and sparsity assumptions. Query algorithms have been developed in [27] and [22] which break the curse of dimensionality through variable reduction and the exploitation of state of the art results from perfect hashing and compressed sensing.

2.1. **Adaptive Partitioning in Sensor Parameter Space.** Highly effective surface reconstructions from point clouds generated by "push-broom" line scanners have been previously developed by project personnel [34]. These algorithms have been based upon ideas from mathematical learning and approximation using adaptive partitions [8, 7, 11]. During this project, USC personnel have implemented the analogue of these algorithms in sensor parameter space with the objective of more accurately adapting the geometry and topology of sensed structures to the point cloud. The estimated range values and corresponding adapted geometry from the sensor-state registered parameter space are then mapped unambiguously to Euclidean world coordinates. This may be incorporated into a larger methodology as on-line updates to the 3D global map, or efficiently time-coded along with sensor state information for later processing. The ranges are estimated over progressively adapted cells in parameter space, going from coarse to fine scales. Cells with no-returns or a small number of unorganized points are then deleted and marked as such. Efforts have focused on reconstructing surfaces from sensed point clouds in which ambiguities between occluded and empty regions cannot be distinguished due to missing, but necessary, information of the sensor lines of sight. Sensor frameworks, such as those being designed and deployed by the VT team of this MURI, typically retain time-coded sensor state information which synchronizes the data streams between multiple sensors and platforms. This added metadata enables fast, unambiguous classification of occupied, non-occupied, and occluded regions, especially when implemented in an adaptively partitioned computational framework.

The natural coordinate system for many classes of ranging sensors is their local (angle,angle) parameter space in which spatial information provided by ranging sensors (e.g. LIDAR, optical, IR, or acoustic) more easily settle what are typically ambiguous spatial questions of point cloud data. These include attributes such as "occupied" versus "non-occupied" surface regions, "interior" versus "exterior" designations for signed distances to surfaces, "occluded" versus "non-occluded" volumetric regions, and "within sensor range and out of range" regions, to name several. Once data is analyzed using this available metadata, it may easily be transformed to update the surface models in global coordinates without ambiguity and providing guidance to fully determine any unsensed regions deemed important to be imaged and resolved. Furthermore, additional properties such as intensity, reflectance, and multiple return waveforms can be encoded for classification and feature analysis, as described in Subsection 2.4 which deals with learning and classification in high dimensions.

Several improvements of the adaptive partitioning in parameter space have been considered and implemented. Both the splitting/merging criteria and the local data fitting have been based on quantities derived from the representation of the data as transformed into a global Cartesian coordinates system, but using the implicitly specified line of sight. The main goal is to distinguish surface segments based upon range estimates which appear in the field of view and to find a good approximation to each surface segment. The adaptive triangular mesh defines neighborhoods around its vertices and corresponding local point clouds representing the neighboring data. For the local fit we consider not only fitting by a single plane (e.g. via principal component analysis) but also analyzing the clustering of the data within the local neighborhood and then fitting it with two (or more) different, near-optimal planar segments. The latter procedure enables the possibility of processing several different surfaces elements with relatively sparse, coarse partitioning and better approximating quality than traditional dyadic splitting. In addition, we analyze appropriate local basis representations using singular value decomposition to process one-dimensional structures and outliers. A PhD student in Mathematics, Kamala Diefenthaler, working under the direction of Peter Binev is preparing the results of this research for publication.

2.2. **Surface registration for improved reconstructions.** Operationally, registration of lidar data collections is necessary for many tasks involved in the assimilation, analysis, interpretation, and extraction of information from point cloud data. For example, airborne data collection typically requires multiple passes over a target region in order to provide a full coverage and to provide different acquisition views to compensate for missing data in the shadow regions due to occlusions. See Figure 6(a)[1], where color corresponds to height. Each pass, or *swath*, is a collection of sample lidar points which should be properly geolocated. Due to inherent errors in positioning of the sensor platform and in the sensor itself, measurements should be aligned on regions of overlap with point cloud swaths from earlier passes. The sensor platform movement, along with its positioning system, introduces complex nonrigid motions and therefore induces highly nonlinear deformations of the data set. These add significantly to the positioning errors of the lidar data points. In the case of airborne lidar acquistion, banking maneuvers of the aircraft are reflected, e.g., in the swath patterns in Figures 6(b) and 6(c).

If there is proper correction of these deformations through nonlinear registration, the overlap regions will have a higher density of sampled points. The result should be finer resolution of the sampled geometry and a resulting higher fidelity in the geometric reconstructions. Moreover, registered multiple passes can detect slowly moving objects within sampled environment, or provide enhanced change detection capabilities. In Figure 6(a) the individual swathes (such as those in Figures 6(b) and 6(c)) were painstakingly post-processed and registered by hand to a common reference frame over a period of months, using rigid motions to compensate for errors in translation and rotation. Although some regions were well-aligned, due to the effects of non-rigid motion and nonlinear distortions, other regions were not. In Figure 7, we have overlaid the two swaths from the Eglin data set, rendering one in green and the second in red. The close-up views of these two data sets from above in Figures 7(a) and from the side in 7(b) show that some geometric features are not aligned, in particular the light pole data circled in blue. This misalignment is due to errors in positioning estimates of the sensor platform by the aircraft's IMU. If the data points from the two swaths are combined and processed by any surface approximation method, clearly the estimation will be unsatisfactory, most likely producing two sets of light poles, or single light pole with poorly reconstructed geometry and oversized by an order of magnitude.

In order to address the nonlinear distortions of positioning in point cloud collections, we describe the current effort which follows our recent work on scanning transmission electron micrographs to formulate the registration as the solution to a nonlinear minimization problem [4]. The process developed there is an involved iterative procedure operating on a sequence of many micrographs. We describe our analogue only in terms of only two swaths, one of which we designate as the *template* data set to which a *reference* data set is to be registered. Although a volume registration analogue can likewise be used for signed distances, we describe only the surface registration version for unsigned distances. First we applied geometric reconstruction algorithms, developed in this MURI program (see e.g. Section 1.2), to each of the swaths to obtain relatively good quality surface fits $\mathcal{S}_1, \mathcal{S}_2 \subset \mathbb{R}^3$ for appropriate subsets within the overlap region of the swaths. If $\mathcal{S}_2$ is fixed as the template surface, the problem then is to determine a deformation $\phi : \mathbb{R}^3 \to \mathbb{R}^3$ such that the surface $\phi(\mathcal{S}_1)$is 'optimally near' the surface $\mathcal{S}_2$. In particular, if $d_{\mathcal{S}_2} : \mathbb{R}^3 \to [0,\infty)$ denotes the unsigned distance to the surface $\mathcal{S}_2$, our idealized matching criterion, i.e. $\phi(\mathcal{S}_1) \subset \mathcal{S}_2$ can then be modeled by finding the ϕ from an appropriate class that minimizes the functional

$$E_{\text{surface}}[\phi] = \int_{\mathcal{S}_1} d_{\mathcal{S}_2}(\phi(x))\, dS(x),$$

[1]Courtesy of *Eglin AFRL/MNG VEAA Data Set #1* by permission

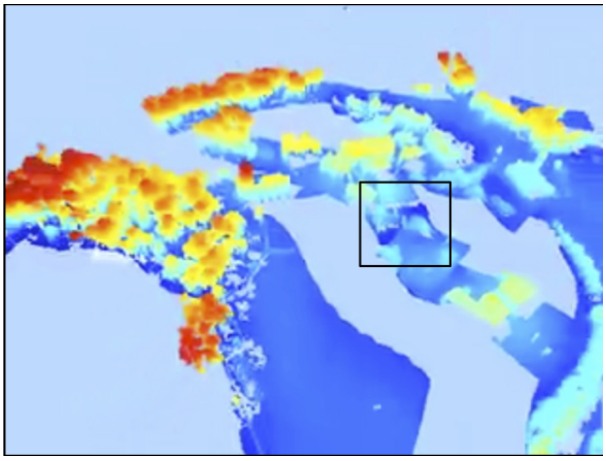

(a)

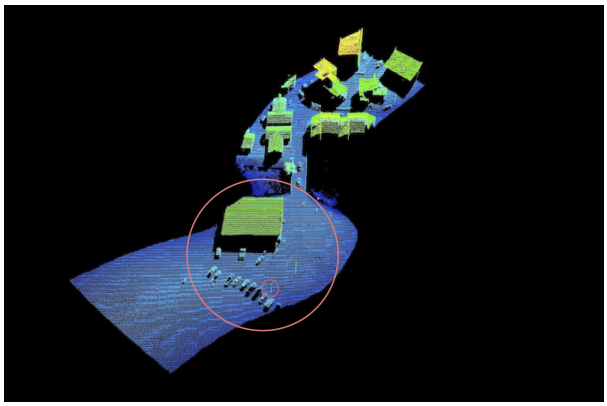

(b)

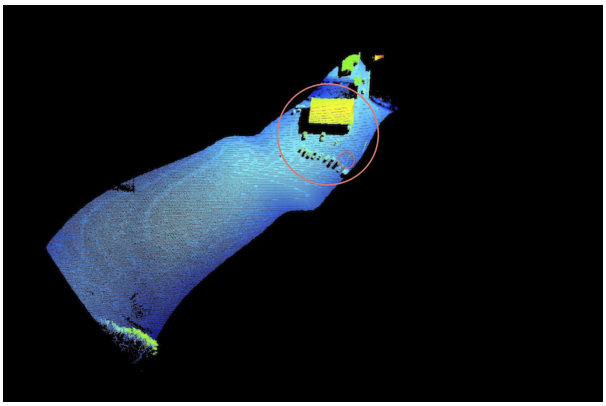

(c)

FIGURE 6. (a) Data swathes representing multiple passes with boxed area indicating one region of overlap. (b) Swath 1 of boxed overlap, (c) Swath 2 of boxed overlap. Note that data is colored by height above bare earth for visual interpretation.

which is effectively an averaged, one-sided Hausdorff distance of the deformation of $\mathcal{S}_1$ to $\mathcal{S}_2$. As a first order registration, we model ϕ using a parametrized rigid body motion, i.e. $\phi[\alpha,\beta,\gamma,t](x) = R_x(\gamma)R_y(\beta)R_z(\alpha)x + t$, where α, β and γ are *yaw, pitch* and *roll* respectively, and $t \in \mathbb{R}^3$ is the translational part of the deformation. The registration problem at this coarse level is solved by minimizing the functional

$$E[\alpha,\beta,\gamma,t] = E_{\text{surface}}[\phi[\alpha,\beta,\gamma,t]]$$

with respect to the deformation parameters. The minimization is a variant of that proposed in [19] performing an explicit, step size controlled gradient descent where the corresponding integrals are evaluated using FEM quadrature approximations for the finite element representation of $\mathcal{S}_1$. This basic procedure is to be used locally at each level from coarse to fine in a multi-level framework to build the nonlinear deformation map ϕ. Figure 8(c) illustrates the effectiveness of the procedure when applied locally to the template and reference patches in Figures 8(a) and 8(b).

If the deformation ϕ is applied to the entire reference swath, the case for nonlocal registration in a multilevel framework becomes clear as seen by the mismatches at other locations. In Figure 9(a)

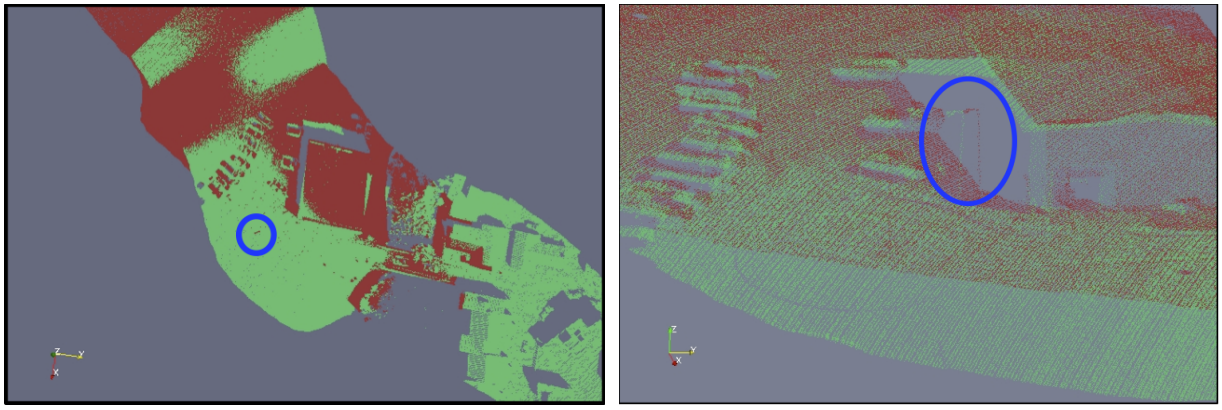

(a) (b)

FIGURE 7. (a) Top view of the two overlaid swaths with lidar point cloud data sensed from a light pole circled in blue, (b) Close up side view of the two point clouds demonstrating a misalignment of the two point clouds around the light pole.

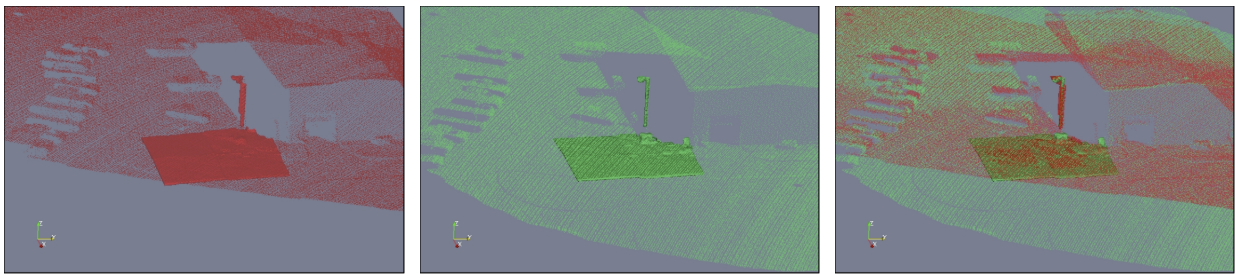

(a) (b) (c)

FIGURE 8. (a) local reconstruction of light pole for template patch, (b) local reconstruction of light pole for reference patch, (c) reference patch registered to template.

where the overlaid registered reference frame is viewed from the side, we see that there is a clear vertical mismatch with substantial separation of 'bare earth' portions between the two swaths. The background light poles on the left side of that figure and the building edges in the upper right of the look-down view of Figure 9(b) show strong nonlinear errors in horizontal positioning.

2.3. **Feature Extraction & Mahalanobis segmentation.** One approach of better analyzing point cloud structure for subsequent surface reconstruction is to decompose the point cloud into segments which may be individually modeled. MURI personnel at South Carolina have developed an orientation invariant, geometric segmentation algorithm, SARG (*Self Adjusting Region Growing*) which organizes point clouds into labeled subclouds whose points share similar features [33] and which are individually are more amenable to reconstruction. SARG is based upon the classical Mahalanobis statistical method for comparison of two normally distributed multivariate distributions and, implicitly, to distinguish outliers. The distance estimation is related to the local Principal Components in that the eigenvectors of the covariance matrix are used as a coordinate system whose corresponding eigenvalues determine the scaling factors for the coordinate directions. The classical Mahalanobis distance from a candidate point P to a set (i.e., labeled segment)

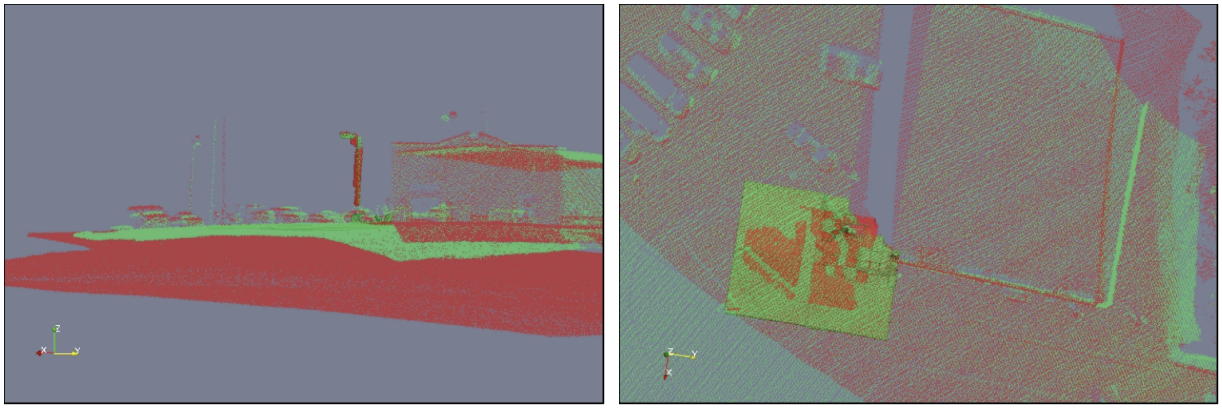

(a) (b)

FIGURE 9. (a) Side view of registered reference swath to template swath, (b) Look down view of same overlaid swaths showing significant nonlinear errors in building edges.

$\mathcal{S} = \{P_1, P_2, \ldots, P_n\} \subset \mathbb{R}^d$ is given by

$$d_M(P,\mathcal{S}) := \sqrt{(P-\mu)^{\mathrm{T}}\,\Sigma^{-1}\,(P-\mu)}, \tag{1}$$

where μ is the center of mass of $\mathcal{S}$ and Σ is the covariance matrix of the collection $\mathcal{S}-\mu$. To accommodate the important cases of vanishing eigenvalues, this definition can be modified by diagonalizing the covariance matrix as $\Sigma = Q\,\Lambda\,Q^{\mathrm{T}}$ where Q is the matrix with eigenvectors as columns arranged according to the corresponding (necessarily nonnegative) eigenvalues $\lambda_1, \ldots, \lambda_d$. The distance formula in (1) may then be generalized and reformulated as

$$d_M(P,\mathcal{S}) := \begin{cases} \sqrt{\Sigma_{j=1}^{j_0} \left(\frac{\tilde{P}_j}{\sqrt{\lambda_j}}\right)^2} & \text{if } \tilde{P}_{j_0+1} = \cdots = \tilde{P}_d = 0, \\ \infty & \text{otherwise,} \end{cases} \tag{2}$$

where j_0 is the number of non-zero eigenvalues of Σ counted with their multiplicities, and $\tilde{P} := (\tilde{P}_1, \ldots, \tilde{P}_d)^{\mathrm{T}} := Q^{\mathrm{T}}(P-\mu)$ are the coordinates of P in the new coordinate system. The SARG algorithm iteratively grows the current segment capturing all points in the cloud which are judged to be close in this distance. The algorithm may be implemented with computational complexity $O(N \log N)$ and has proved effective for several fielded scanning, flash, and burst illumination lidar systems See, for example, Figures 10-11 below. Similar results were obtained for data obtained by the Virginia Tech dual axis lidar system and were presented during the Year 2 review.

In Figures 10 a)-d), the SARG algorithm is applied to scanning LIDAR data provided by NATO SET118 collaborators from the Defense Research and Development Canada - Valcartier for selected testing of MURI algoritms. Image a) depicts the original LIDAR point cloud. Image b) is a rendering of the SARG-segmented subclouds labeled by various colors, with Person 2 colored as magenta. A multiresolution surface reconstruction is shown for these two subclouds in Figures 10 c)-d), respectively. Higher quality reconstructions are provided in Figure 17 using UC-I's three dimensional binary image segmentation formulation described in Section 4.2.

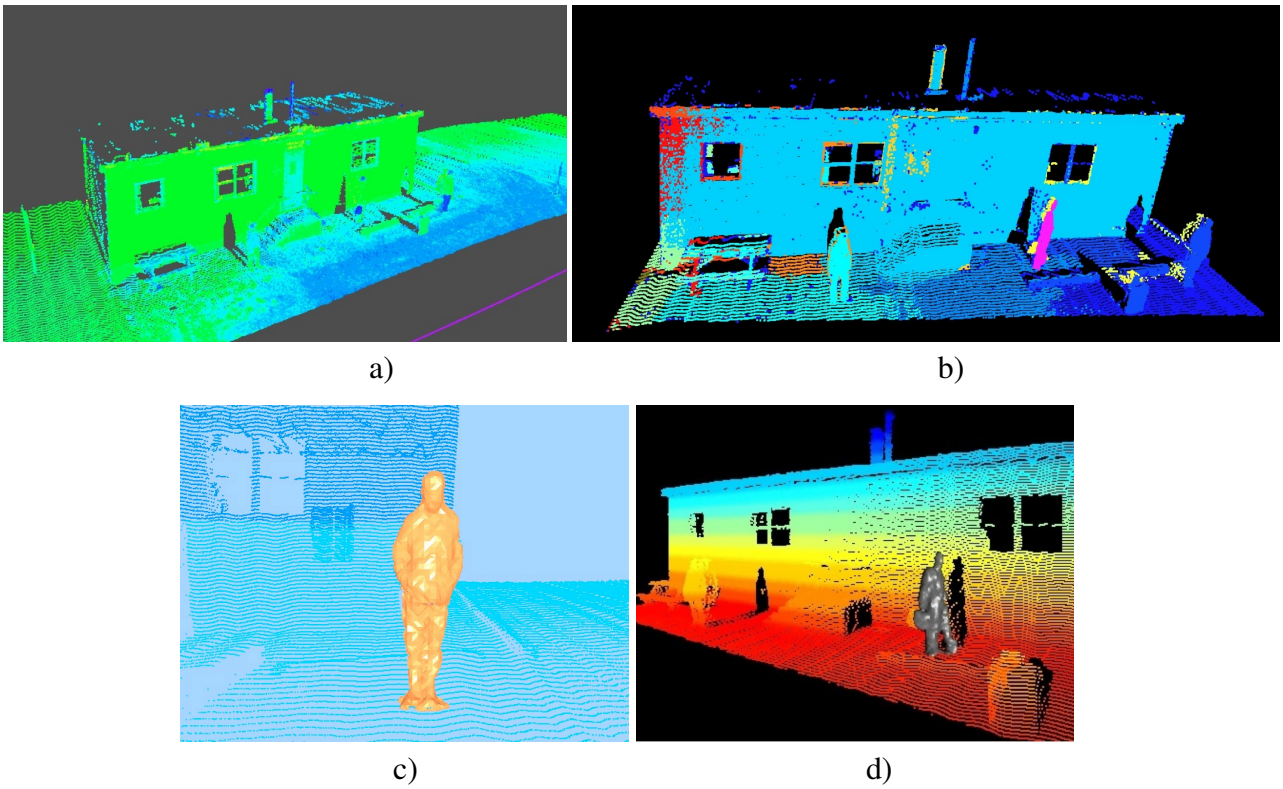

FIGURE 10. Iterated Mahalanobis segmentation of scanning LIDAR data provided by DRDC-Valcartier NATO SET118 collaboration. a) LIDAR Point Cloud; b) segmented subclouds labeled by color; c) surface reconstruction for person 1; d) surface reconstruction for person 2.

Figures 11 a)-f) presents the results of SARG applied to burst illumination LIDAR data provided by NATO SET118 collaborators from the Defence Science and Technology Laboratory (UK Ministry of Defence). Figure 11 a) is a photo of the imaged scene, with parts b)-c) representing side and front views of the sign in the foreground. In these images magenta used to color the residual set after the iterated segmentation. Figure 11 d) is a rendering of the surfaces constructed from the segmented sub-clouds along with the original data. Figures 11 e)-f) show similar views from the side and front for the vehicle in the background of the photo in part a).

The SARG algorithm is naturally suited for implementation in CUDA for GPU (Graphical Processing Units) which will compensate for its more expensive $O(N \log N)$ performance to enable its potential for real-time processing on small platforms. Other known bottlenecks, although still linear in computational complexity, have previously been implemented in CUDA, including multiresolution PCA, complex wavelets, and the chamfer algorithm for estimating the Hausdorff metric. Speedups of forty or more have been achieved for these algorithms on standard graphics processors, but requires a careful study of algorithm design for memory management.

2.4. **High Dimensional Learning and Classification.** In many application domains of mathematical learning, point cloud data can be viewed as random independent draws of some unknown probability distribution ρ and problems are formulated as ones of either regression or classification. Classification problems are key to resolving several practical issues that emerge in processing point

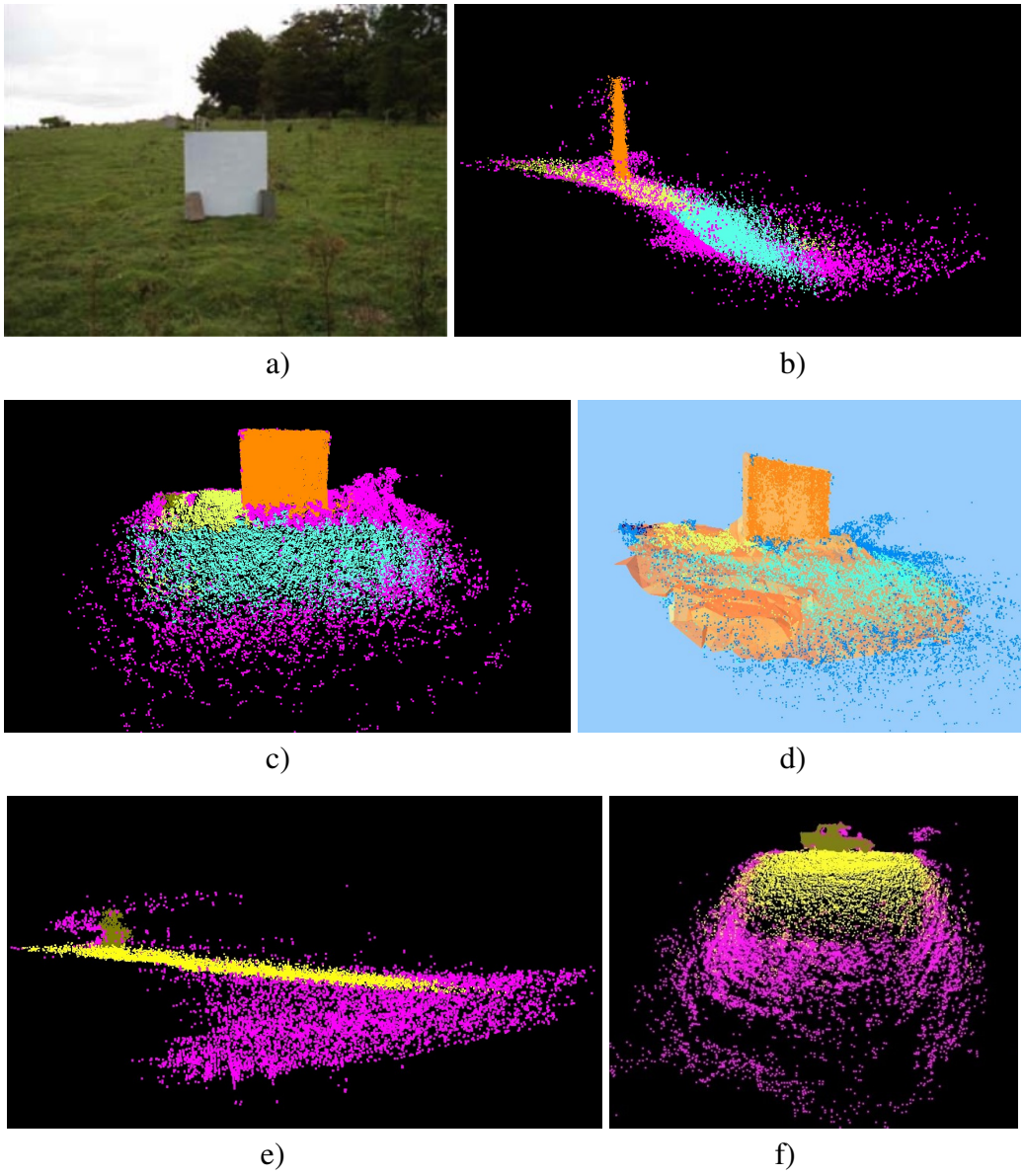

FIGURE 11. Iterated Mahalanobis segmentation applied to 3D burst illumination LIDAR data provided by Dstl-UK NATO SET118 collaboration. a) Photo of test scene with target sign in foreground and vehicle in background; b) side view of segmented subclouds around target sign with 'noise label' magenta ; c) front view of segmented subclouds around target sign; d) reconstructed surfaces around target along with point cloud; e) side view of background vehicle; f) front view of background vehicle.

clouds and, in particular, problems on extracting embedded information from urban terrain data. The development of a theory to provide quantifiable estimates of the probability of classification, based upon minimization of a risk functional, is therefore extremely important for decision makers and in the design of reliable classification algorithms.

We are developing new theory and algorithms for classification directed at high dimensional problems, such as

- the analysis of chemical-biological gas plume concentration levels moving through an urban environment imaged by frequency agile lidar (FAR) measurements. Here by processing a set of observations, e.g. spatial/temporal multichannel spectral measurements, the goal of classification of the chem-bio agents is aimed so that false alarms of threats are reduced while incurring very low risk.

- classification of conventional lidar point clouds by signatures (based on geometry, topology, reflectance, distribution of multiple returns) into sets designated as either man-made structures (including buildings, roadways, bridges, power lines, walls, or vehicles) or natural features (such as waterways or vegetation). The classification geometric "signatures" may be used for relational database queries to determine possible candidate locations within a region for a designated object of interest.

In these example cases, each of the observations detects several characteristics of objects. The vector of these characteristics can be considered as a point in a high dimensional space X. Based on some additional knowledge, the objects and their corresponding points from X are grouped in classes. The classification problem processes the preliminary (training) observations in such a way that for every new query from X we are able to predict its class with preassigned high confidence. Typically, the outcome is considered $+1$ if the point is from a designated class of interest and -1 otherwise. Ideally, we can assume that the observations are independent drawings from a probability measure ρ over the cross product of the space X with $Y := \{+1, -1\}$. If for a given point x from X we define $\eta(x) = E(y|x)$ as the expectation of y given x, then the best classifier, called the Bayes classifier, is given by the set Q^* of all points x from X for which the expected value $\eta(x)$ of the outcome is positive. By assigning $+1$ to the points from Q^* and -1 for the ones outside, the measure $R(Q^*)$ of the misclassified points, called the risk, is minimized.

The goal of the empirical classification algorithms is to find a good approximation Q to the set Q^* using a limited variety of approximating sets. Given a family F of subsets of X, we consider the square of the expected value of the outcomes for a set S from this family. If this quantity is larger than t times the measure of S, the set S is called *t-reliable*. For sufficiently large t, this property guaranties that the prediction based on the empirical estimates for the sign of the outcomes on the set S will be correct with high probability.

Our theoretical analysis involves the smoothness properties of the regression function η around the boundary of Q^*. This allows us to construct an adaptive procedure for building the family F of approximating sets that does not use explicitly knowledge about this smoothness. We denote by η_S the integral of η over a subset S of X with respect to the measure ρ_X induced by ρ on X. By ρ_S we denote the amount of this measure on the set S. Then, the t-reliability is expressed by $|\eta_S|^2 \geq t\, \rho_S$. If the sets S are the building blocks used to assemble the family F, then it is important to limit the influence of the sets that are not t-reliable. One particular line of investigation is to find a setup in which the total measure of the unreliable sets can be reduced. In the case that we have a complete knowledge of ρ, this could be done easily by building a family F that resolves well the boundary of Q^*. In general, we do not have any information about ρ and one can build F based on the assumption that ρ has certain properties. An example for such an assumption is the Tsybakov noise condition that requires that the measure of the set of all x from X, for which $|\eta(x)| \leq \delta$ is limited by a constant times the q-th power of δ. Many classification algorithms are theoretically validated based on estimates assuming this condition. However, it is designed primarily for reducing the

total risk $R(Q)$ of the approximating set Q. Since this risk cannot be below $R(Q^*)$, the actual goal should be to find conditions under which the excess risk $R(Q) - R(Q^*)$ would be reduced. This motivates our investigations to design a different theoretical setup aiming at incorporating such conditions and by this to enlarge the set of measures ρ for which it applies. Our main tool is a specific modulus $\omega(\rho, \varepsilon)$ that analyzes the variance term for a given classification algorithm. The threshold parameter $\varepsilon = \varepsilon(S)$ is designed to estimate the error of the empirical approximation of η_S. It can be adjusted to provide estimates based on Tsybakov noise condition but other choices give more general results, in particular for $\eta(x)$ belonging to smoothness classes similar to ones defined by Besov spaces.

Motivated by the above mentioned theoretical findings we design partition-based empirical algorithms for classification. Some of the advantages of our procedure include its online data assimilating capabilities and fast computation.

We build a full binary tree corresponding to adaptive partition rules using the paradigm of sparse occupancy trees [10] to handle the data. Given a specific t, we then find through a thinning process the finest possible partition P such that for each leaf node in the corresponding tree, either it or its sibling is part of a t-reliable set S. The set S can be a cell of the current partition or union of several adjacent cells from it. In the case of simplicial partitions we can choose the sets S to be the simplices from the current partition adjacent to a vertex. Once the partition P is found, we calculate empirical estimates for the local excess risk at each node of its tree going fine-to-course and assuming that the excess risk is 0 at the leaf nodes. Based on these estimates we then find a near-best tree approximation P^* of the partition for Q^* with $m = m(t)$ elements. Since m is an increasing function of t, we can adjust t, based on the comparison of the trees for P and P^*, to avoid underfitting or overfitting. The set Q is then defined as a union of all cells S of P^* with $\eta_S \geq 0$. This algorithm is universal in the sense that it does not assume any prior knowledge of the smoothness of $\eta(x)$. In addition, one can be more conservative in forming the set Q and only include cells S with $\eta_S > 0$ that are part of reliable sets reducing the potential of false positives.

This new theory and algorithms which exploits occupancy trees and new models for high dimensional functions has been developed for classification in [5]. These algorithms have provable high order convergence under margin conditions and sparsity assumptions.

Query algorithms have also been developed in [27] and [22] which break the curse of dimensionality through variable-reduction and the exploitation of state of the art results from perfect hashing and compressed sensing.

3. Estimation and Approximation from Sensor Networks

As imaging sensors have become more compact over the past decade, there has been increasing interest in deriving estimation and approximation specifically for classes of sensor networks. During the last year, the MURI team has continued to investigate how the approximation and learning theoretic approaches developed by the team can be extended to this important class of problems. Significant progress has been made through the collaboration of Princeton University, Virginia Tech, the University of South Carolina and Texas A&M University.

Over the past year, the efforts at Princeton in support of this MURI have been in the broad area of distributed learning and pattern recognition. The Princeton team of the MURI has focused on the following two problems: (1) semi-supervised consensus segmentation and (2) distributed sensor localization.

3.1. **Graphical Models for Distributed Learning.** Reproducing kernel methods are a popular and highly successful approach to nonparametric learning and pattern recognition. These methods takes as input a training set $\cup_{j=1}^{m} S_i = S = \{(X_i, Y_i)\}_{i=1}^{m}$ and in the least-squares regression setting output a function $f_\lambda : \mathcal{X} \to \mathcal{Y}$ which solves the optimization problem

$$\min_{f \in \mathcal{H}_K} \left[\sum_{i=1}^{m} (f(X_i) - Y_i)^2 + \lambda \|f\|^2_{\mathcal{H}_K} \right]. \tag{3}$$

Here, $\mathcal{H}_K$ is a reproducing kernel Hilbert space to which the regression function is constrained to belong. This space is induced by a kernel function $K(\cdot,\cdot)$, and the minimizer $f_\lambda \in \mathcal{H}_K$ of the optimization problem can be written in the form

$$f_\lambda(\cdot) = \sum_{i=1}^{m} c_{\lambda,i} K(\cdot, X_i) \tag{4}$$

Solving the optimization problem is difficult in distributed settings with resource constraints, when there are a collection of sensors, each observing an example (X_i, Y_i). We have explored methods for solving this problem that relies on local (and iterative) sharing of data, not entire functions, and thereby addresses the practical weakness that sometimes limits the applicability of other methods (e.g., the incremental subgradient approach).

In this approach, each sensor i queries its neighbors' data and uses this local data to compute a global estimate for the field by solving

$$\min_{f \in \mathcal{H}_K} \left[\sum_{j \in N_i} (f(X_j) - Y_j)^2 + \lambda_i \|f\|^2_{\mathcal{H}_K} \right]. \tag{5}$$

We can iterate through the network allowing each sensor to compute a global estimate using only local data. The key idea for propagating information is to couple this iterative process using a set of message variables. Multiple passes through the network are made. The resulting algorithm is depicted pictorially in the figure below.

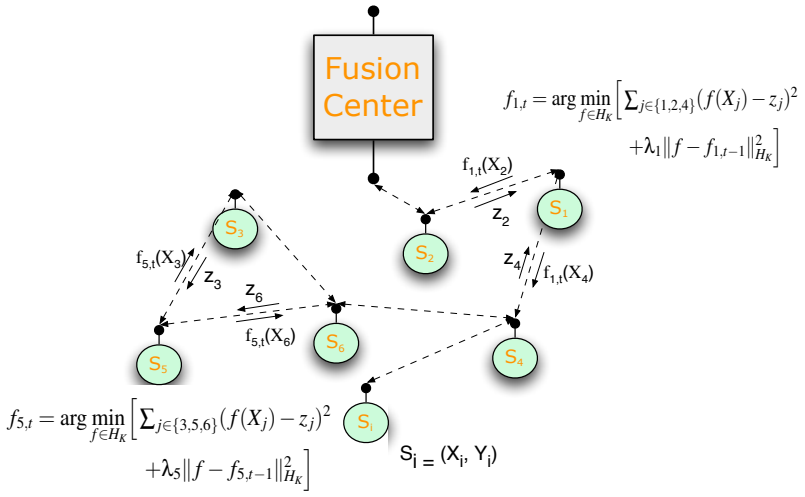

FIGURE 12. Training Distributively with Alternating Projections

This approach is inspired by methods from graphical models, belief propagation, message-passing, etc. The approach is independent of assumptions that couple the kernel $K(\cdot,\cdot)$ with the network topology. Thus, prior domain knowledge about $\mathbf{P}_{XY}$ (the joint distribution of (X,Y)) can

be encoded in the kernel; the training algorithm approximates the centralized estimator as closely as the communication constraints allow. Secondly, sensors only share estimates of functions at a small number of points, and not the functions themselves. This significantly broadens the scope of problems where the approach is applicable. During this MURI, we made contributions to this approach to distributed learning and pattern recognition in a variety of ways.

3.2. **Semi-supervised Consensus Clustering and Segmentation.** We developed a new method for learning how to achieve consensus among several segmentation outputs. The suggested method employs prior information about the target objects to be detected after the segmentation step in order to learn the distance metrics and the weight parameters of classical consensus clustering algorithms.

Initially, several segmentation algorithms are used independently with different parameter sets as base segmentation algorithms to segment the remote sensing images. Then, the segmented images are fused in order to reach a consensus on the sets. The proposed method, called Semisupervised Consensus Clustering, is based on the classical Filtered Stochastic Best One-Element-Move (BOEM) algorithm. This method is reformulated to incorporate the prior information to semi-supervise the consensus clustering process. For this purpose, we employ must-link and must-not-link constraints in the optimization problem.

We, also, define and compute the partition weights in Filtered Stochastic BOEM. Finally, we suggest a learning method to enhance the distance function and algorithm parameters. We have applied our new semisupervised consensus segmentation method to the segmentation of hyperspectral and aerial remote sensing images. We have studied the consensus on the segmentation outputs of k-Means, Normalized Cuts, Graph Cuts and Meanshift algorithms.

3.3. **Aggregating Probabilistic Forecasts.** We have continued our efforts to develop methods for combining forecasts of probability of complex, interrelated events from multiple forecasters. Low level algorithms can be utilized to provide probability forecasts for a broad range of events. Our techniques provide a means for fusing this information for higher level processing. With a large number of sensors and even larger number of events, one of the main challenges is to find computationally feasible algorithms. We have developed methods based on alternating projections that provide excellent results in reasonable time.

As part of this MURI, we developed a new algorithm for combining probabilistic assessments from a large pool of judges, with the goal of efficiently implementing the Coherent Approximation Principle (CAP) while weighting judges by their credibility. We introduced two measures of a judge's likely credibility, and we used these to determine the judge's weight in aggregation. The algorithm was applied to a dataset of nearly half a million probability estimates of events related to the 2008 US presidential election (over 16000 judges). Compared with simple scalable CAP algorithms, our schemes improved the stochastic accuracy with a comparable run time, demonstrating the effectiveness of the weighting methods for aggregating large numbers and varieties of forecasts. Also, we found that smart weighting allows particular subsets of events to be aggregated more accurately and comparison with probabilistic predictions from popular prediction markets and poll aggregators showed excellent performance of the weighted CAP algorithms.

We investigated two further methods to improve the forecasting accuracy within the CAP framework and developed practical algorithms for these. These methods allow flexibility to add fixed constraints to the coherentization process and to compensate for the psychological bias present in probability estimates from human judges. The algorithms were tested on the election data set and

the results showed that both methods improve the stochastic accuracy of the aggregated forecasts compared to using simple CAP.

3.4. **Geometric Estimation.** We investigated several problems in geometric estimation. That is, given an underlying geometric object (shape, surface, trajectory, etc.), we are interested in estimating the object given different forms of noisy measurements. In particular, we studied shape/surface/trajectory reconstruction based on point cloud data (potentially with time stamps) in a noisy environment.

We developed a noise resistant ellipse/spheroid fitting algorithm with an innovative objective function. Our method provides more accurate axial direction estimation in noisy environments. We combined this new objective function with an efficient iterative algorithm with a correction term so that it can obtain accurate axial estimation as well as accurate fitting of the size of the ellipse/spheroid.

To better deal with outliers in ellipse fitting, and more generally, in curve and surface fitting, we developed a hybrid outlier detection algorithm combining both proximity-based and model-based outlier detection techniques. Our hybrid technique can effectively eliminate outliers of various types, and considerably improves the robustness of ellipse/spheroid fitting for scenarios with a large proportions of outliers and high levels of inlier noise.

A third problem we considered in this area is joint to shape and trajectory reconstruction of rigid bodies from distributively collected, asynchronous point cloud data with time stamps. We developed an energy-minimization scheme is to solve the trajectory reconstruction problem of rigid bodies with known shape parameters, assuming that the rigid body moves in an energy efficient manner with an acceleration upper limit. We generalized this basic method is to the case with unknown rigid body shape parameters, employing cross-validation techniques to determine the best parameter hypothesis.

3.5. **Distributed Sensor Localization.** Localization is an essential tool in many sensor network applications. Over the years, a rich literature has been developed to solve the sensor localization problem from different perspectives. Four criteria are anchor-based vs. anchor free, incremental vs. concurrent, fine-grained vs. coarse-grained, and centralized vs. distributed. The spring model algorithm we have developed is a distributed, concurrent, fine-grained algorithm to solve the sensor localization problems. We have focused on an anchor-based scenario so as to obtain absolute coordinates of the sensors in the network. Our central ideas are composed of three techniques to improve the spring model algorithm for solving localization problems in a wireless sensor network with anchors.

First, we solve the two-dimensional localization problem in a three-dimensional space. This dimension expansion technique can effectively prevent the spring model algorithm from falling into local minima.

Second, the Hooke spring force (linear force, or quadratic potential) is generalized to spring with an L_p potential function. The optimality of different values of p is compared under different noise environments. Our simulation results show that $p = 2$, i.e. Hooke force, is good choice of spring for Gaussian noise, yet for Laplacian noise, $p = 1.3$ outperforms other choices of Lp potential functions.

Third, we introduce a customized spring force function with "lock-in" mode, which has larger strength when the estimated distance between two sensors is close to the true length of the spring, is introduced, which accelerates the convergence speed of the algorithm.

All these techniques significantly improve the noise resistance and efficiency of the spring model algorithm. We demonstrated the efficacy of these algorithms by multiple simulations, especially in a scenario with anchor points of longer broadcasting radius than other sensors.

3.6. **Consensus and Approximation Theory.** Building on the historical contributions of Princeton in decentralized optimization, researchers at Virginia Tech have concentrated during the last year on extending their results using the approximation theoretic results obtained by the University of South Carolina and Texas A&M University.

3.6.1. *The Global Optimization Problem.* We consider a network of n vehicles labeled $i = 1 \dots n$ whose communication connectivity is described by a graph $\mathcal{G} := \{\mathcal{V}, \mathcal{E}\}$ where $\mathcal{V}$ denotes the nodes and $\mathcal{E}$ defines the edges in the graph. Individual vehicle nodes may be airborne, marine or terrestrial. We suppose each vehicle i collects *local* measurements $\mathbf{z}^i = \{(x_k^i, y_k^i)\}_{k \in \mathbb{Z}^+}$ over time steps $k = 1, 2, \dots$, that represent some problem specific external field f of interest. Several assumptions on the measurement processes and network communication motivate the research in this proposal. We assume that (A1) the measurement processes have extremely high bandwidth measured in bits per second, (A2) the communication bandwidth over the channels described by the graph $\mathcal{G}$ is insufficient to share the measurement data in real time, (A3) the computing and storage capacity of each node is limited, and (A4) the desired behavior of the network or collective can be expressed in terms of some globally defined cost or loss function $\mathcal{J}$. The loss or performance function $\mathcal{J}$ depends on the observations by all agents $\boldsymbol{z} := \{\boldsymbol{z}^1, \boldsymbol{z}^2, \dots, \boldsymbol{z}^n\}$, or is approximated by an empirical loss function $\mathcal{J}_{\boldsymbol{z}}$ that depends on the observations. In either case, we suppress the dependency on the observations $\boldsymbol{z}$ in the discussion that follows. The data that is collected by the network is to be used to find the solution of the infinite dimensional, distributed optimization problem where we seek the collection of estimates $\boldsymbol{f}^* := \{f^{*1}, \dots, f^{*n}\} \in \boldsymbol{H}$ that solves the optimization problem

$$\boldsymbol{f}^* = \underset{\boldsymbol{f} \in \boldsymbol{H}, \mathbf{B}(\boldsymbol{f}) = 0}{\operatorname{argmin}} \ \mathcal{J}(\boldsymbol{f})$$

where $\boldsymbol{H} := \mathcal{H}^1 \times \cdots \times \mathcal{H}^n$ is the hypothesis space of admissible agent solutions, $\mathcal{J}$ is the loss or cost function to be minimized and $\mathbf{B}(\boldsymbol{f})$ encodes the constraints imposed among the solutions achieved by the agents. The constraint operator, for example, can impose conditions that enforce communication compatibility as dictated by the connectivity graph $\mathcal{G}$. Numerous applications of interest to the Army including distributed exploration and mapping, mine detection, hazard detection, distributed path planning and multivehicle control can be expressed in the form above for distributed vehicle teams.

3.6.2. *Local Problems and the Learning Dynamic.* Our general approach to the solution of the above global optimization problem uses the vehicle team to construct a distributed computing system that generates successive approximations that converge to the global solution. In our strategy the network of agents construct a sequence of approximations of the original optimization problem via a two stage learning dynamic. In this dynamic, the agents use their most recent data to solve local optimization problems and subsequently update these local solutions using functionals that depend on the shared data. At time step $t_k \in \mathbb{R}^+$ during the *local optimization stage*, each agent i constructs a local optimal estimate $\hat{f}_k^i$ that is the solution to

$$\hat{f}_k^i := \underset{f^i \in \mathcal{H}^i}{\operatorname{argmin}} \ \mathcal{J}_k^i(f^i)$$

where $\mathcal{J}_k^i(\cdot)$ is a local cost function. Once the local optimal estimates $\hat{\boldsymbol{f}}_k := \{\hat{f}_k^1, \hat{f}_k^2, \ldots, \hat{f}_k^n\}$ have been generated, shared information functionals $\boldsymbol{p}_k := \boldsymbol{p}_k(\hat{\boldsymbol{f}}_k)$ are constructed which define information that is communicated over the network. Finally, during the *communication sharing and update stage*, each agent constructs its final estimate at time step $t_k \in \mathbb{R}^+$ using its current local estimate $\hat{f}_k^i$ and the shared information functionals

$$f_k^i := T_k^i(\hat{f}_k^i, \boldsymbol{p}_k)$$

where $T_k^i(\cdot)$ is a nonlinear update operator.

The two-stage learning dynamic above, which is described in more detail in [23, 24], is quite general in structure. Several questions are addressed in our research. The first question regards the convergence of the final collection of estimates to the solution of the global optimization problem

$$\boldsymbol{f}_k := \{f_k^1, \ldots, f_k^n\} \to \boldsymbol{f}^* := \{f^{1,*}, \ldots, f^{n,*}\} \tag{6}$$

Many different authors have studied sufficient conditions for convergence in Equation 6 in the special case that $\boldsymbol{f}_k$ evolves in some finite dimensional space. The focus of our study is the selection of appropriate, infinite dimensional approximation spaces for evolution of the sequence of estimates $\{\boldsymbol{f}_k\}_{k\in\mathbb{N}}$. This viewpoint has two important implications. The first is that synthesis of techniques from approximation theory as outlined in [8, 25] enables the derivation of *rates of convergence* that are optimal up to a logarithmic term. These estimates have no counterpart in methods that assume *a priori* that estimates evolve in a finite dimensional space. The second implication is that powerful methods for compression, encoding and decoding of shared information are obtained. These methods provide a rigorous and systematic method for modulating the bandwidth of communication across the network. This can be a critical feature in applications to autonomous vehicle networks where communication bandwidth is extremely limited.

3.6.3. *Progress in Consensus Estimation in Infinite dimensional Spaces.* The general strategy above has been successfully developed by the authors with extremely promising preliminary results. By developing the framework for consensus approximation as a distribution free learning problem, the solution of the problem is achieved via a distributed optimization of a collective error function subject to consensus constraints. This approach is novel and noteworthy in the following respects:

(1) The consensus estimation problem is posed as a distributed optimization problem among agents in (infinite dimensional) approximation spaces.
(2) The decentralized optimization problem is construed as a stochastic optimization problem where the probability distributions that characterize agent sampling, as well as the smoothness or approximation properties of the unknown function, are not known *a priori*.
(3) The theoretical framework naturally lends itself to compression, encoding and decoding of the shared information functionals. The parsimonious exchange of information among nodes can be critical to severely bandwidth limited autonomous military vehicles.
(4) The theoretical framework enables the derivation of optimal rates of convergence for a class of popular loss functions, up to a logarithmic factor, for a wide range of approximation spaces.
(5) Highly efficient multigrid methods have been derived for implementation of the methodology based on techniques originating in multilevel optimization and numerical methods for partial differential equations.

Further details of this approach can be found in the references [23, 24, 8, 25].

4. Implicit Geometric Representations and Operations

During the MURI project, the UCI team has focused on processing and analysis of point clouds and implicit surface reconstruction from point clouds that can be very useful for 3D modeling of terrain from LiDAR measurements. In particular we have achieved the following:

- Robust and accurate point cloud normal estimation, denoising and segmentation.
- Efficient and robust implicit surface reconstruction for point clouds based on convexified image segmentation.
- Analysis and understanding of point clouds using geometric partial differential equation (PDE).

The UCI teams has collaborated with their counterparts at Texas A&M and the University of South Carolina to provide accurate and efficient normal estimation for streaming surface reconstruction using wavelets. Methods for point cloud segmentation and implicit surface reconstruction have been combined with visibility of point clouds and exploratory path planning algorithms developed by the University of Texas and UCLA. Below is a brief summary of these results.

4.1. **Robust and accurate point cloud normal estimation, denoising and segmentation.** Surface normal approximation is an important but challenging task that is utilized by several applications including reconstruction, estimating local feature size, computer aided design (CAD), and inside-outside queries. The UCI team has developed an improved surface normal approximation method, based on recasting the popular principal component analysis formulation as a constrained least squares problem in [16]. The new approach is robust to singularities in the data, such as intersecting planes, and also incorporates data denoising. Principal component analysis (PCA) is a popular method for computing surface normal approximations from point cloud data. The PCA normal approximation is accurate when the underlying surface is smooth, but tends to smear across singularities, such as corners or intersecting planes. The smearing is caused by the contribution of data points from across the singularity. Figure 13 illustrates this phenomenon.

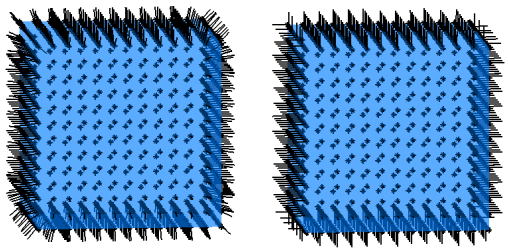

FIGURE 13. PCA normal estimation for a cube. Left: Standard PCA. Notice the smeared normals along the edges of the cube. Right: Nonlinear least squares normal estimation.

The PCA normal approximation can also be described as the solution to the following constrained least squares problem:

$$\begin{aligned} \min_{\eta} \quad & \tfrac{1}{2}\|V\eta\|_2^2 \\ \text{s.t.} \quad & \|\eta\| = 1, \end{aligned} \tag{7}$$

where the rows of the matrix $V \in R^{K\times 3}$ are the difference vectors $v_k = x_k - \bar{p}$. The equality constraint is necessary to ensure a nontrivial solution.

In order to reduce the contribution of points from across the singularity, the approach incorporates an adaptive weighting term designed to deflate such contributions. The result is the following constrained nonlinear least squares formulation:

$$\begin{aligned} \min_{\eta} \quad & \tfrac{1}{2}\sum_{k=1}^{K}\left[e^{-\lambda(a_k^T\eta)^2}(a_k^T\eta)\right]^2 \\ \text{s.t.} \quad & \|\eta\| = 1. \end{aligned} \tag{8}$$

Traditional weighting terms place emphasis on proximity, and also serve as a window function which isolates the local neighbors. The weighting term $e^{-\lambda(a_k^T\eta)^2}$ adaptively deflates the contribution of terms with high orthogonality mismatch at a rate defined by the parameter λ. Naturally, setting λ to zero results in the original PCA linear least squares problem 7, with the exception that the difference vectors are taken from the data point p and not the centroid $\bar{p}$. The equality constraint is easily absorbed into the objective function by representing the unknown surface normal η in spherical coordinates. Applying formulation 8 to the box data results in significant improvement in the surface normal estimates, as illustrated by Figure 13.

Dealing with noise in LiDAR data is another important issue. Investigators at UCI have incorporated noise robustness into normal estimation in their work. Based on robust and accurate normal estimation, they also have developed a simple segmentation scheme for point clouds that can decompose a point cloud into disconnected components and/or pieces with similar normals by constructing a symmetric adjacency matrix for the point cloud. Figure 14 shows an example of segmenting different buildings directly from point clouds.

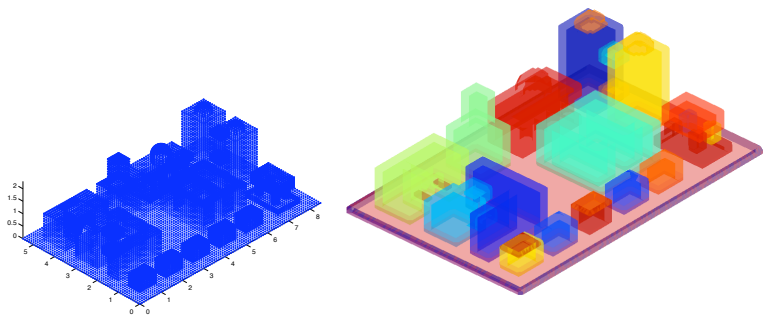

FIGURE 14. Direct segmentation of point cloud.

4.2. **Efficient and robust implicit surface reconstruction for point clouds based on convexified image segmentation.** The main advantage of using implicit representations is the flexibility and robustness in dealing with complicated topology and the automatic representation of holes or gaps in surface reconstruction. Implicit representations also allow one to generate distance fields which are useful for estimation of the Hausdorff metric, autonomous navigation, line of sight calculations and other operations. The implicit representation can be easily fed into implicit wavelet representation developed by MURI groups at University of South Carolina and Texas A&M University.

In the work [42] UCI investigators formulate the implicit surface reconstruction for point clouds as a three dimensional binary image segmentation problem. In particular the technique utilizes recent convexified image segmentation models and efficient convex optimization techniques in the formulation. One of the convexified image segmentation models the team has adopted is the TVG-L1 model:

$$\min_{u} \int_{\Omega} g(x)|\nabla u(x)| + \lambda|u-f|dx. \tag{9}$$

In the first term, $g(x) > 0$ is an edge indicator function which is close to zero at edge locations. This term alone is akin to the geodesic active contour model. For example, if $u(x)$ is a characteristic function, then $\int_{\Omega} g(x)|\nabla u(x)|$ is the weighted (by $g(x)$) length/area of the boundary by the co-area formula for total variation (TV). The second term is a volumetric image fitting term in which f is the given image. When $g(x) = 1$ and f is a binary image, it can be shown that a global minimizer of (9) is equivalent to a global minimizer Σ of the non-convex variational problem (for binary image defined by Ω):

$$\min_{\Sigma} |\partial\Sigma| + \lambda|\Sigma \triangle \Omega|, \tag{10}$$

where $\triangle$ denoting the symmetric differences of the two sets. Another closely related binary image segmentation model we used is the following CVG model,

$$\min_{0\le u\le 1, c_1, c_2} \int_{\Omega} g(x)|\nabla u(x)| + \lambda\left[(f-c_1)^2 - (f-c_2)^2\right] u(x)dx. \tag{11}$$

Here, $g(x)$ and $f(x)$ are exactly as in the TV-L1 setting, and c_1 and c_2 are two constants.

However, different from standard image segmentation where an initial image uniformly sampled on a rectangular grid is given, two key issues are (1) there is no initial image f given on a regular grid, and (2) a good edge indicator $g(x)$ needs to be constructed. Researchers in the UCI team have developed novel ways to construct this information directly from the scattered point clouds.

To construct an initial image that can provide a good indication of inside and outside regions, they use a consistent normal estimation developed earlier in this MURI project [16] and incorporates volumetric information, such as line of sight. To construct a sharp edge indicator that can provide a accurate data fitting term that is robust to noise UCI uses a superposition of anisotropic Gaussian kernels where the direction and anisotropy are defined based on local principal component analysis (PCA). Below, a few numerical results are provided that show both efficiency and robustness of the proposed method in the construction of water tight surfaces for PCÕs with complicated topology, noise, and holes. A comparison of the method is given with the most popular and state of the art implicit surface reconstruction algorithm, Poisson surface reconstruction, proposed in [46].

Figures 15 and 16 show the ability of the method to fill holes or gaps in the data. Figure 17 shows the reconstruction from highly non-uniform and sparse LiDAR data.

4.3. **Analysis and understanding of point clouds using geometric PDEs.** Point clouds provide a basic and intrinsic way of sampling and representing geometric objects in 3D modeling as well as conveying information in higher dimensions. Local linear approximations, such as generated by PCA, can only reveal local structure. Understanding or characterizing global structure is a very challenging task. By analyzing the properties of geometric intrinsic differential operators one can obtain global information about the underlying geometry. The UCI team has developed a general framework and computational methods for solving geometric partial differential equations on point clouds in 3D and higher dimensions [43, 41, 35]. The discrete approximation of differential operators on the underlying manifold represented by point clouds is based only on local reconstruction, which is simple, efficient and accurate. In particular, using global differential operators, such as the Laplace-Beltrami (LB) operator, one can link local reconstruction to a global manifold structure

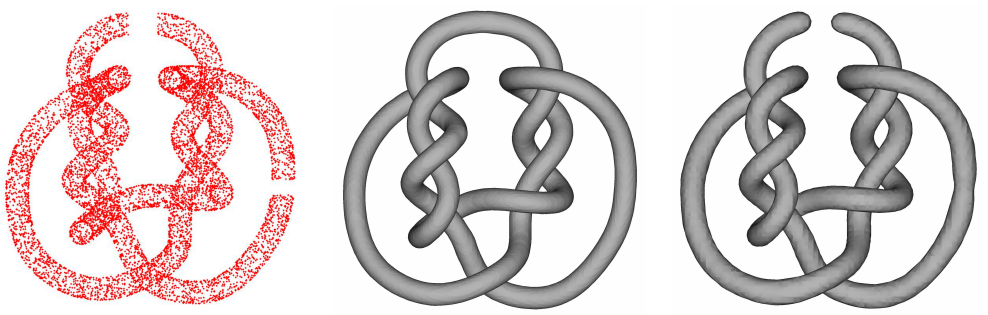

(a) (b) (c)

FIGURE 15. (a) knot with gaps. (b) is our reconstructed surface. (c) is result of Poisson surface reconstruction.

and extract intrinsic geometric information of the point cloud. The framework extends to manifolds of any (co-)dimension with or without boundary. The complexity of our method scales well with the total number of points and the true dimension of the manifold, not the embedded dimension. Another important application of our method is in data science, where the task of visualizing, extracting information, analyzing and inferring underlying structure from data samples is ubiquitous. In many cases, point cloud data resides or is believed to reside on or near a low-dimensional manifold in a much higher dimensional ambient space. Although there are useful tools, such as the principal component analysis (PCA) to provide local dimension and linear approximations of structure, it is very challenging to extract global information and to understand structure in general. Mathematically and computationally one can gain intrinsic information by studying the behavior of differential equations, such as the heat equation or the eigenvalue problem for differential operators such as Laplace-Beltrami operator, on manifolds.

The framework developed by UCI in [43, 41, 35] solves PDEs directly on point clouds without using parametrization, triangulation or grid, which can be difficult to construct in general and may introduce artifacts. The key idea is that one can define differential operators on a manifold by local construction of the manifold. In another word, once we can construct a function as well as the manifold locally in a common reference coordinate, we can differentiate the function with respect to the metric of the underlying manifold simply using the chain rule. So in our method, we only need to use the K-nearest neighbor (KNN) points to define a local intrinsic coordinate system using PCA and to construct the manifold and function locally using least squares. Local approximation error and super-convergence results have been studied in [43] and applications to geometric understanding of point clouds have been presented in [41].

Here we present experiments (see Figures 18-21) for the demonstration of computing heat kernels, distance maps and geodesics on points clouds, computing eigenvalues and eigenfunctions for Laplace-Beltrami operators, and registration between point clouds using shape descriptors based on eigensystems of the Laplace operator that are invariant under isometric deformations and scaling.

4.4. **3-D Nonlocal Total Variation (NLTV) Methods:** Typical lidar systems transmit a laser pulse and receive a deluge of data in the form of a point cloud. This point cloud contains important information reflected from the scene of interest, and can be quite voluminous. As a result it challenges current reconstruction methods and storage capabilities. Further, the sensitivity of the photo-detectors (e.g.,Geiger-mode avalanche photodiodes) can generate significant noise.

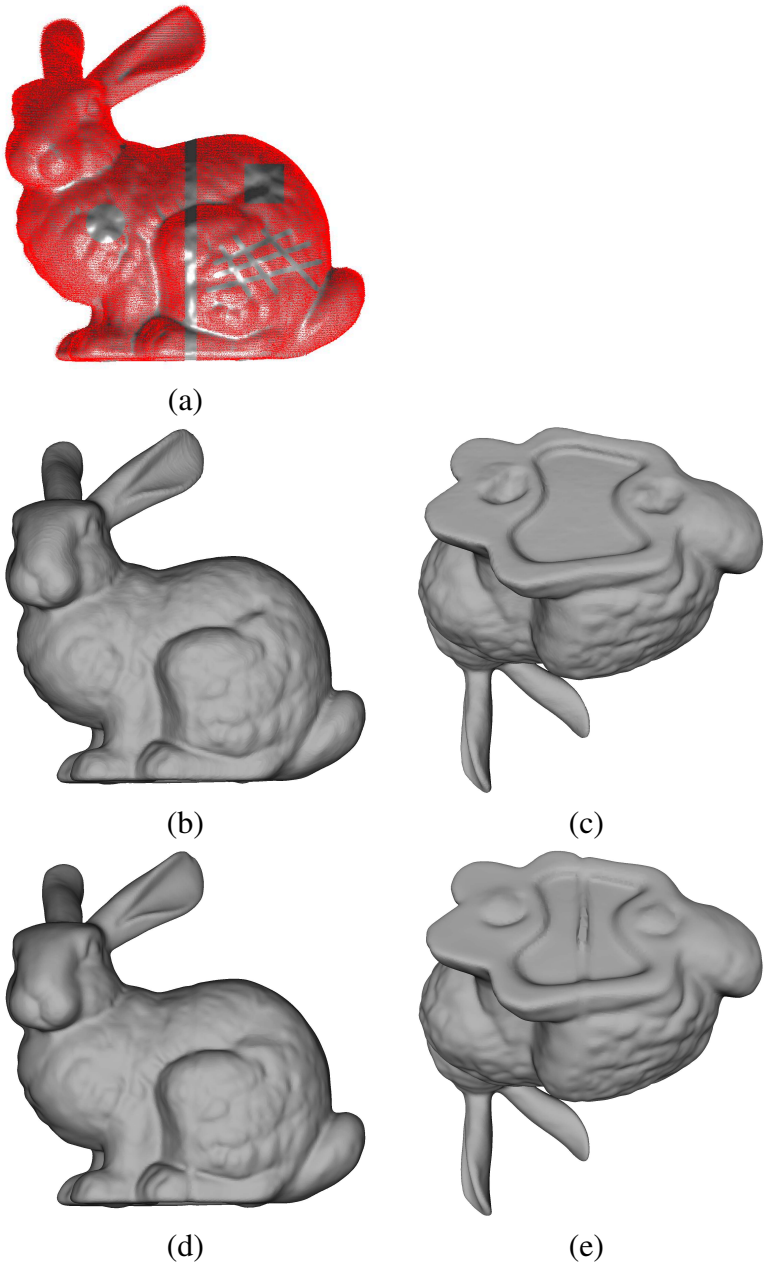

FIGURE 16. (a) bunny with holes, (b) & (c) is our reconstructed surface. (d) & (e) is result of Poisson surface reconstruction.

Current state-of-the-art three-dimensional surface reconstruction algorithms require the use of a grid to determine measures of gradient and proximity of points. However, forcing data points onto a grid can result in a loss of subtle geometric information inherent in the scene.

Over the past year, researchers at UCLA have initiated work on a 3-D grid-free, generalization of regularization with non-local methods, which are already used extensively to denoise 2-D images. The technique examines 3-D "cloud patches" and tries to find similar geometric characteristics. By minimizing the nonlocal total variation (NLTV) between these characteristics the method is able to significantly denoise a 3-D cloud data set. We briefly overview this method. Essentially, the

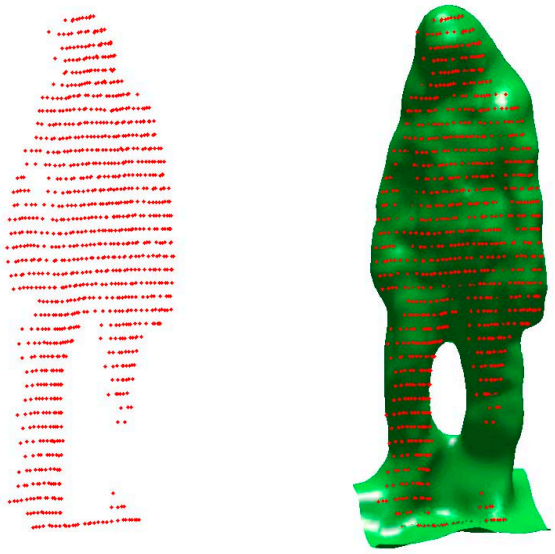

(a) LiDAR data (b) implicit surface reconstruction

FIGURE 17

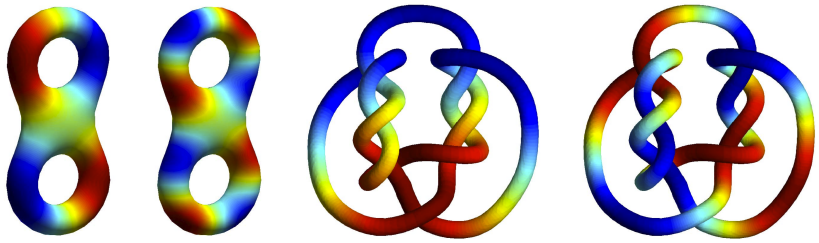

FIGURE 18. eigenfunctions of Laplace-Beltrami operator on point clouds

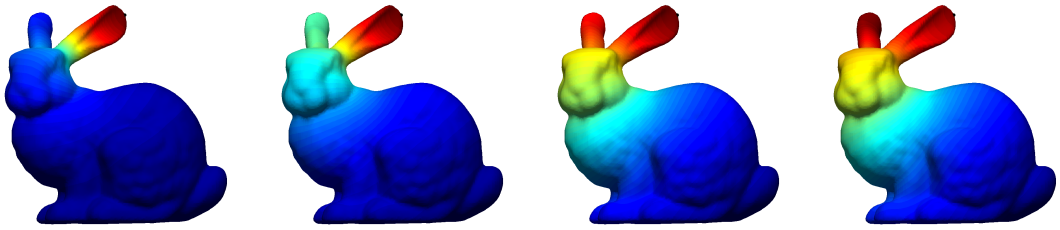

FIGURE 19. Heat kernel on point cloud

method seeks to use the unique geometry of individual patch clouds to identify specific structures. If p and q denote two points in the point cloud data, a patch cloud about p or q is defined in terms of its k nearest neighbors. The characteristic $\mathcal{C}_f(p) := p - \overline{p}$ is defined for each patch cloud by subtracting the centroid $\overline{p}$. It is apparent that the characteristic $\mathcal{C}_f(p)$ is analogous to the intensity of a pixel in a 2-D image. After normalization, the geometry description $\mathcal{G}(p)$ is used to describe the geometry in the vicinity of the point p, and a nonlocal measure of similarity between two patch

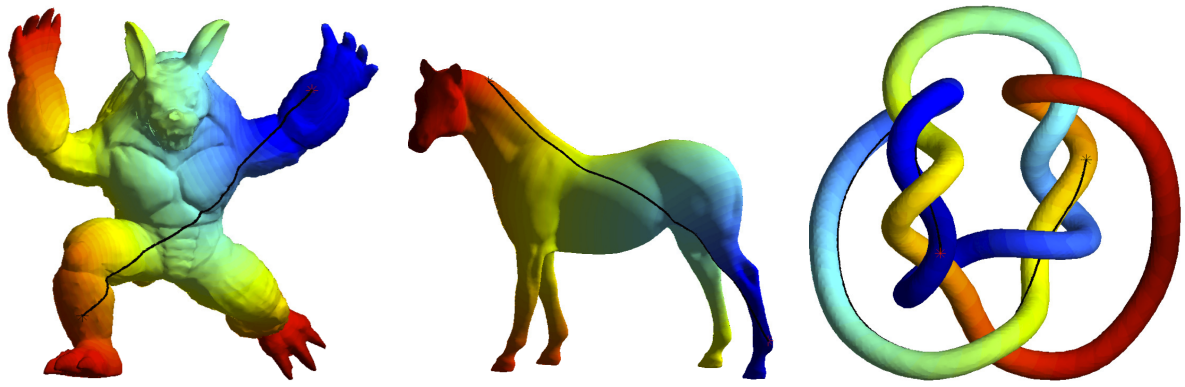

FIGURE 20. Distance maps and geodesics on point clouds

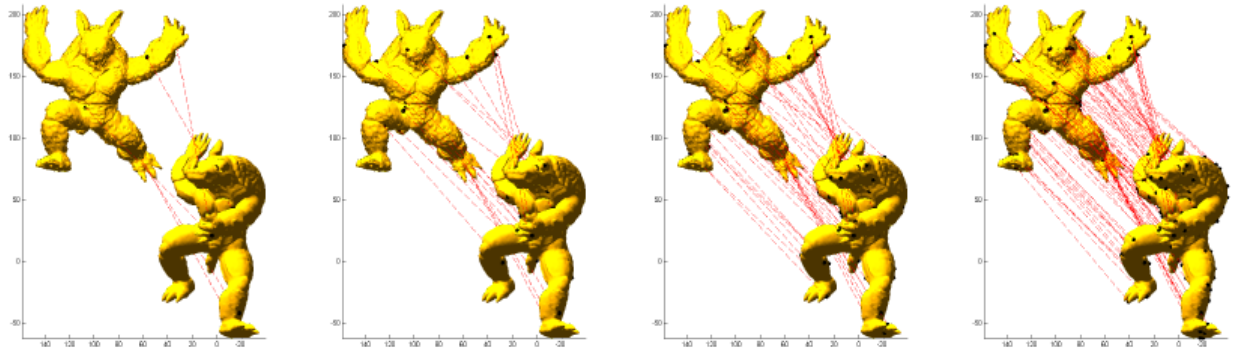

FIGURE 21. Registration of point clouds (with noise).

clouds centered at p and q is given by the weight function $w_f(p,q)$ defined as

$$w_f(p,q) := \frac{1}{Z_p} e^{-\frac{\|\mathcal{G}_f(q)-\mathcal{G}_f(p)\|_2^2}{h^2}}$$

Finally, denoising is achieved by solving either the minimization in terms of the L_2 norm,

$$\min_u \left(\int \mu |\nabla_w u| + \frac{1}{2}\|u-f\|_2^2 \right)$$

or the minimization in terms of the L_1 norm,

$$\min_u \left(\int \mu |\nabla_w u| + \frac{1}{2}\|u-f\|_1 \right)$$

where the operate ∇_w is defined as

$$(\nabla_w u)(p,q) := (C_u(q) - C_u(p)) \sqrt{w_f(p,q)}$$

The simulated images below show a noisy scene on the left, and the denoised version using our algorithm in the center and on the right. Notice that changing codimension presents no difficulties.

The approach lends itself to the efficient design of point cloud dictionaries which can lead to multiscale sparse reconstruction of noisy images and has led to truly remarkable denoising in the level set representation of interpolating implicit surfaces.

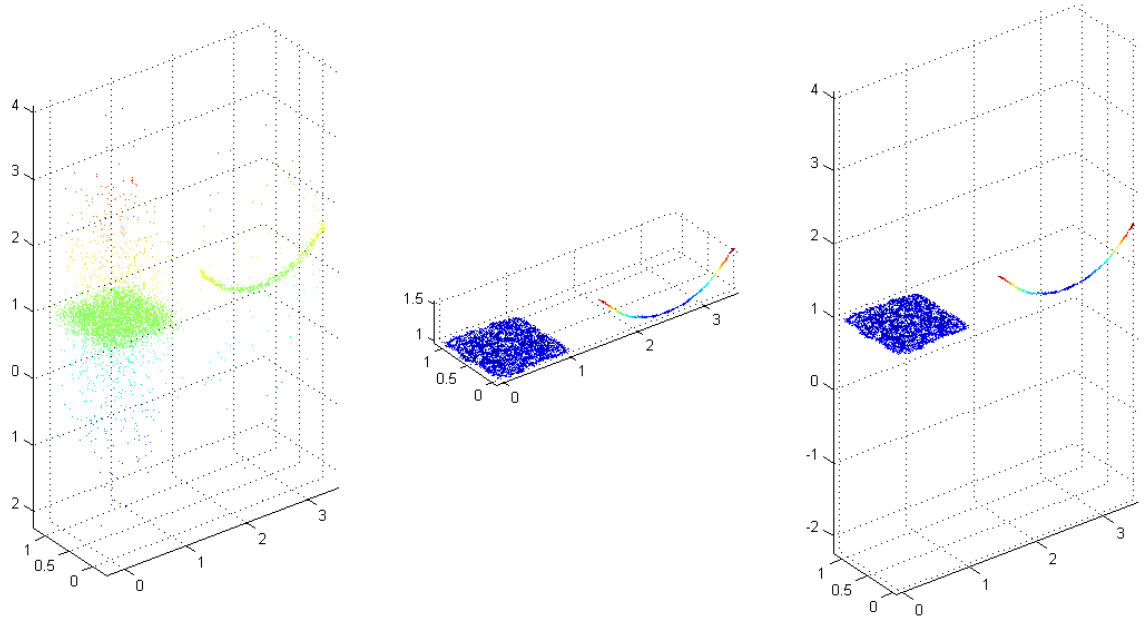

FIGURE 22. NLTV Denoising Example. Left: Noised corrupted geometry including filamentary structure. Right: Denoised geometry obtained via NLTV

4.5. **Change Detection and Surveillance.** Figure 23 shows a single frame of a video surveillance stream from a parking lot at the Adelphi Army base. The upper left shows the scene with 40 % randomly chosen missing points. The upper right figure depicts the difference between two successive frames. The lower left frame is the result of application of the robust PCA algorithm of [14]. This method uses L_1 theory to find the sparse component (background) and the nuclear norm to find the low rank component (motion). Our method, devised in [29], uses the tight frame decomposition of [13], minimizing the L_1 sum of the coefficients. These results are extremely promising and suggest new avenues for achieving state-of-the-art surveillance.

4.6. **A Fast Convex Optimization Method for Surface Reconstruction.** In [28] we developed a method for distance preservation in level set evolution which is very fast, using the split Bregman algorithm of Goldstein and Osher [31]. We reduce surface interpolation to a total variation minimization problem, as in [30] which involves a redistancing step. The final results are state-of-the-art in speed and are quite accurate. See Figures 24-27

In [36] we developed a splitting method based again on Bregman iteration for optimization with orthogonality constraints. This is a nonconvex problem but we use analytic solutions in the nonconvex minimization step. We obtain state-of-the-art results for conformal mapping for surface construction, direction fields correction and noisy color image restoration. See Figures 28- 30.

FIGURE 23. Video tracking with 50% missing data: new fast method allows tracking Very noisy environment.

FIGURE 24. Proposed level set-based segmentation method applied to natural images. For each result, we show the segmentation result and the level set function. We plot the initial zero level set in blue, the final contour in pink and the $\pm 1, \pm 2$ level sets of the final functions in black

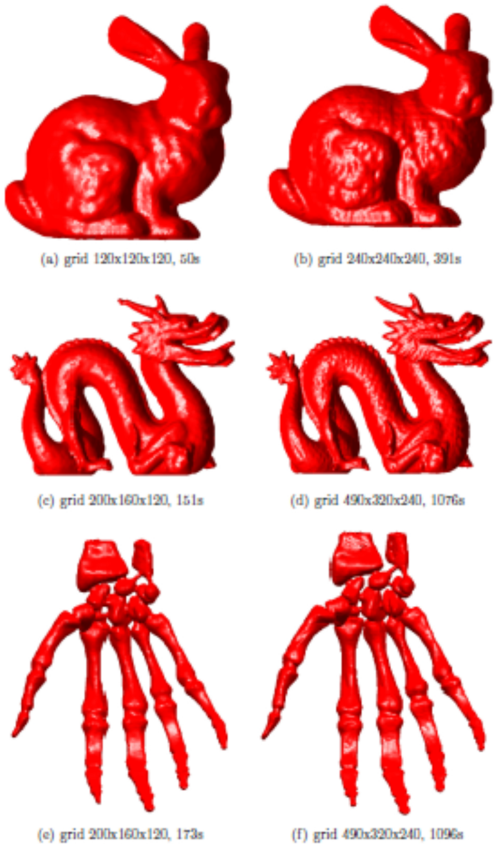

FIGURE 25. Reconstructed surfaces from scattered data points at different resolutions

FIGURE 26. Reconstructed surfaces from scattered data points at different resolutions

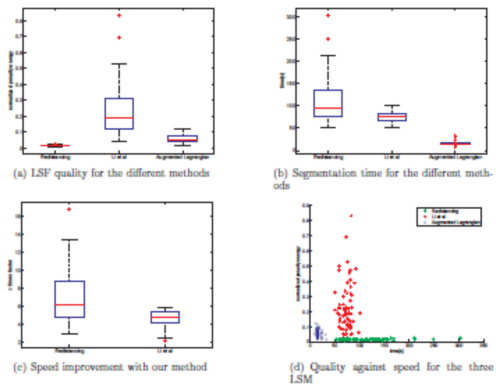

(a) LSF quality for the different methods (b) Segmentation time for the different methods (c) Speed improvement with our method (d) Quality against speed for the three LSM

FIGURE 27. Comparison of quality of segmentation and speed for the different methods on a dataset of 72 images. Quality of the LSF is measured in terms of the penalty term at convergence $\frac{1}{|\Omega|}\int(|\nabla\phi|-1)^2$ when the obtained contours are equivalent. Our method preserves the SDF almost as well as redistancing, clearly better than Li *et al.*'s method and is faster than any of them.

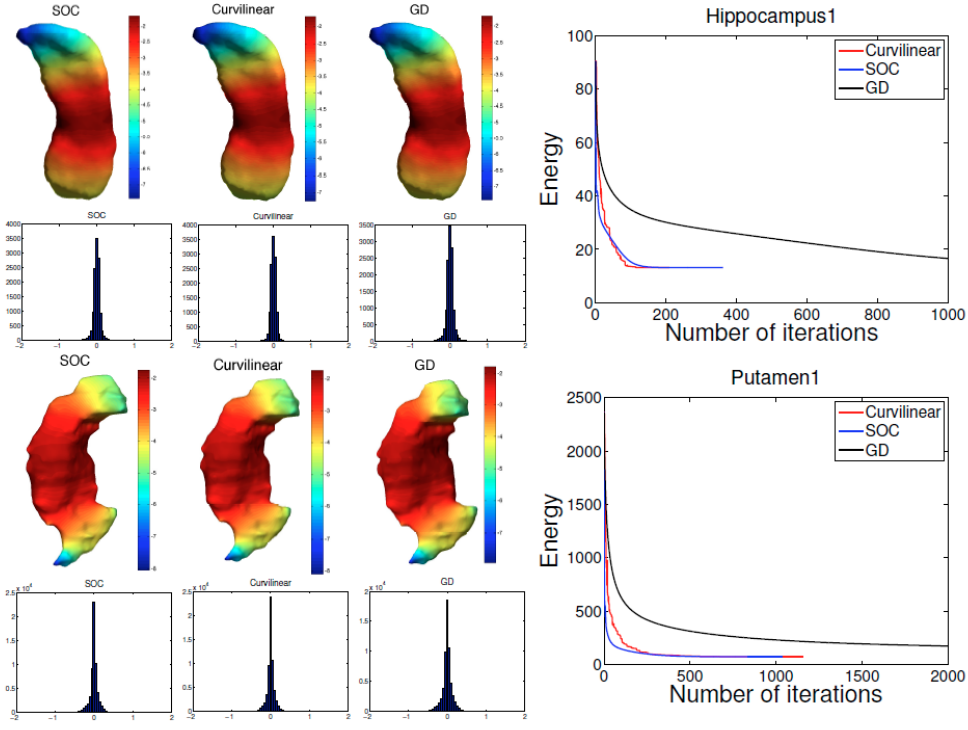

FIGURE 28. Comparison of the proposed algorithm with the curvilinear algorithm and the gradient descent method. Surfaces are coded by the conformal factors obtained from the resulting conformal mappings. Histograms show angle difference between triangles on the input surface $\mathcal{M}$ and the corresponding triangles on the obtained map. The last column illustrates the energy evolution via iteration numbers.

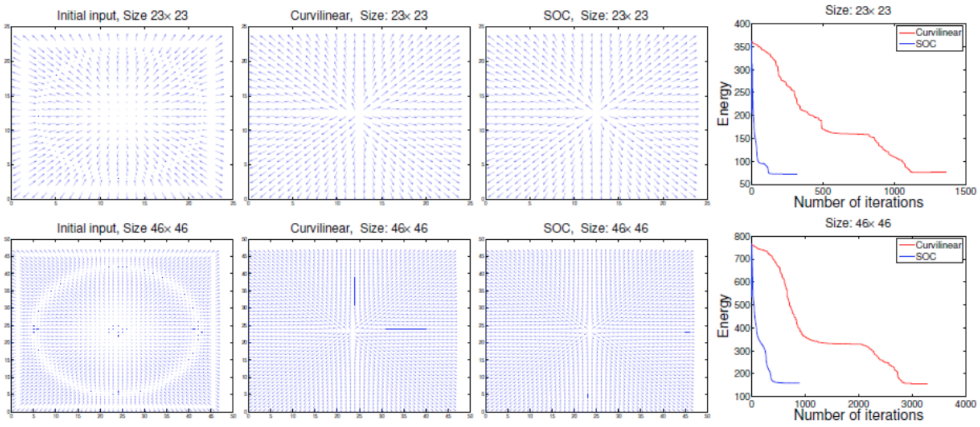

FIGURE 29. Comparison between the proposed algorithm and the curvilinear search algorithm. The first column shows the initial inputs $\overset{\rightarrow}{\mathbf{F}}^{0}$ for both algorithms. The second and the third columns are the results obtained from the curvilinear algorithm and our proposed *SOC* algorithm, respectively. The last column illustrates the energy evolution via the iteration numbers.

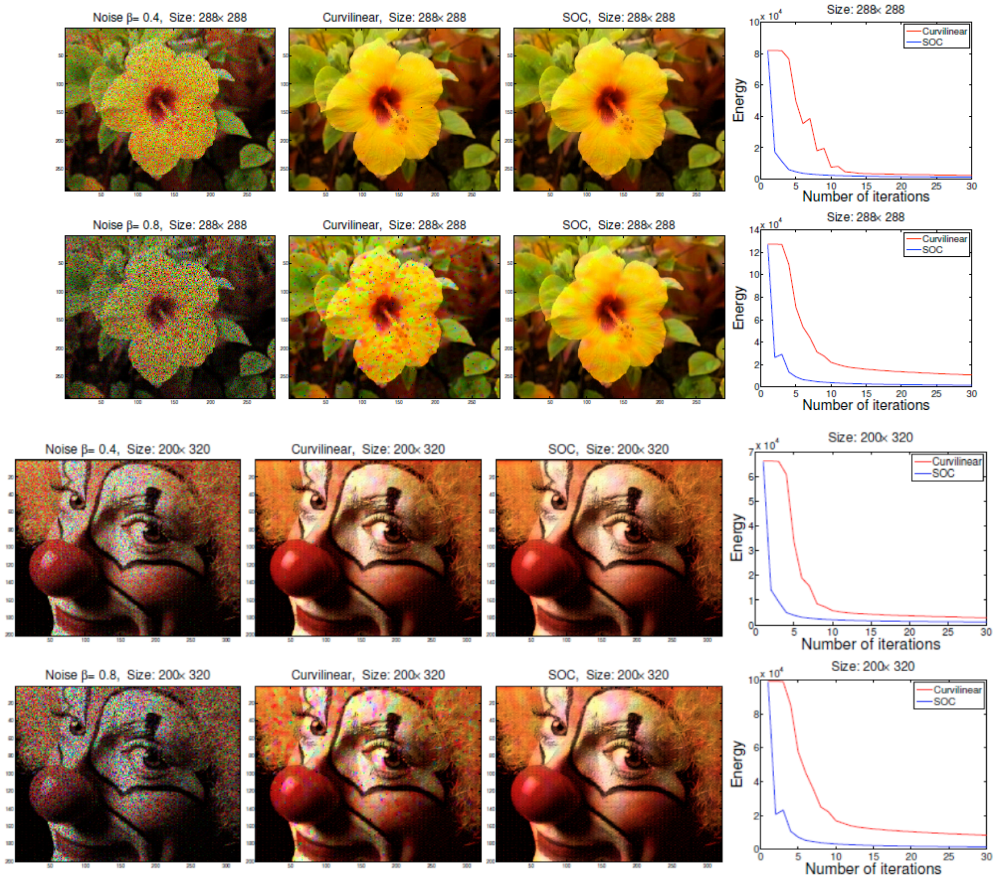

FIGURE 30. Comparison between the proposed algorithm and the curvilinear algorithm with fixed 30 iterations. The first column shows the input images contaminated by two different levels of Gaussian noise on their chromaticity. The second and the third columns are results obtained from the curvilinear algorithms and our proposed *SOC* algorithm, respectively. The last column illustrates the energy evolution via iteration numbers.

5. VISIBILITY OF POINT CLOUDS AND APPLICATIONS TO PATH PLANNING PROBLEMS

The problem of visibility seeks to determine the regions in space visible to a given set of observers in the presence of occlusions. UT along with its collaborators, TAMU, Univ. South Carolina and UCLA, have been developing algorithms that reconstruct visible surfaces of the occluding objects based on the point cloud data sampled from the opaque objects in the environment. The MURI team members have been working on applying the developed point cloud reconstruction algorithms to the problem of exploring environments with complicated and unknown obstacles using single or multiple observers. As a result of the exploration, a complete map of the environment is obtained. A convergence proof [39] has been provided indicating suitability of the proposed algorithm for some general types of environments. Various post-processing optimization techniques may be considered to obtain a more uniform exposure of the environment along the path.

In the point cloud database, there are structures such as overpasses and multi-story, perhaps irregular, buildings that pose additional challenges for the previously developed algorithms. During the final year of this project, following the feedback of Year 4 government review, we have been developing new visibility-based "non-myopic" exploration algorithms for the fully 3D cases. The essential building block consists of a class of functionals, hereafter referred to as visibility "metrics", that **quantifies the potential gain in new visibility information** by placing a new observing location at certain designated locations, given the previous observing locations.

Below, we briefly outline the our mathematical and algorithmic approaches. We first list the essential ingredients in defining such type of metrics:

- **The set of observing locations** O: The metric will depends on the visibility from a set of observing locations contained in $O = \{x_1, \cdots, x_k\}$.
- **The obstacles** Ω: They are assumed to be a closed set containing finite number of connected components.
- **Occlusion set** $\mathcal{S}$: The occlusion set contains points that are not visible from (the observing locations in) O. When the visibility from O encompasses the entirety of the domain except the obstacles, then the occlusion set is identical to the obstacles. In this case, we shall say that the observing locations in O have ***complete visibility*** of the domain.
- **Shadow boundary** $\partial\mathcal{S}$: A hyper-surface which separates the domain locally into visible and occluded regions. The shadow boundary is the attenuation of the visible portions of the obstacles along the lines-of-sight. Note that the visible portions of the obstacles are not counted as part of the shadow boundary.
- **The portion of shadow boundary that is visible to** z **will be denoted by** $\mathcal{S}_z$.
- **Viewing angle** θ: This is the angle between the line-of-sight that reaches the shadow boundary and the normal of the shadow boundary at the intersection.
  The viewing angle penalizes viewing the shadow boundary by grazing through it. It also reflects on the uncertainties due to errors in the visibility information. The closer this angle is to 90° , the more sensitive the view will be to perturbation in the obstacles.
- **Depth of occlusion** τ**:** We associate each point on the shadow boundary with a *depth* which reflects on the thickness of the occlusion set in the direction that is orthogonal to the shadow boundary.
  The depth value quantifies the volume of occlusion set that can become visible if a vantage point looks perpendicularly at a point on the shadow boundary.
- **The weighting** w**:** Additional weighting may be placed over the entire domain for additional application-specific modeling needs, such as prioritization of a subset of the domain or dealing with visibility with limited range.

With all these ingredients, we define the metric as a boundary integral taking the following form:

$$\mu(z;O) := \int_{\partial\mathcal{S}_z} w(z,O)\tau(y)\theta(z,y)dS(y) = \int_{\partial\mathcal{S}_z} (w\tau\,\vec{r}_z)\cdot\vec{n}\,dS(y). \tag{12}$$

Here $\vec{r}_z(y)$ is $(z-y)/|z-y|$ the viewing vector.

Figure 31 demonstrates a visibility metric in 2D following the above formulation. In the left subfigure, the observing location is shown by the diamond shape, the obstacles are the two circles shown in blue. The red curves show the shadow boundary and the portions of the circles that are visible to the observing location. The right subfigure shows the values of $\mu(z;(1,0.25)^T)$. The values increase from blue to red.

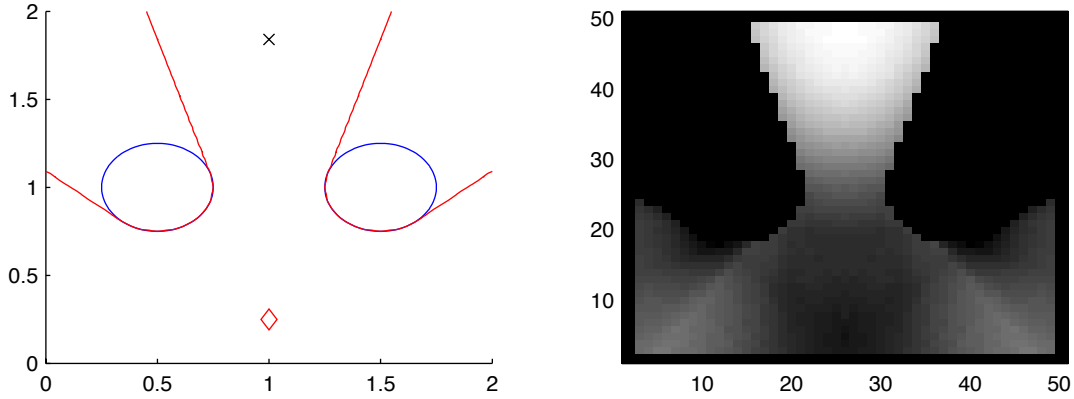

FIGURE 31. The values of a visibility metric defined in (12) in a domain containing two circles. The cross shows where the metric is maximum.

We consider the problem of planning a path through an unknown environment that contains complicated geometry; the objective of such path is to map out the environment using suitable technologies such as the online multi-resolution point cloud algorithm that is developed by this MURI project. We solve this problem by constructing a sequence of observing locations, $x_0, x_1, \cdots, x_k$, and a path that goes through these locations. The *k-th* observing location, x_k, will be chosen according to a *visibility metric*, using information obtained from the observing locations $x_0, \cdots x_{k-1}$. Figure 32 demonstrates a step-by-step computer simulation using this technique. Figure 33 shows a simulation result for a more complicated set up. We point out here that this procedure is *transparent to the dimension of the problem* – the construction of the observing locations depend solely on the visibility metric, which does not require any dimension specific logic. Indeed, the initial 3D implementation of the proposed visibility metric in our navigation strategy produced very promising results for regular building-like structures as shown in Figure 34, where we performed simulations using four buildings.

Furthermore, it is conceivable that in certain applications, one is interested in mapping out certain part of the domain sooner than the other parts. The goal to "put some region under surveillance sooner" translates into the objective of having visibility on that region using as few observing locations as possible, starting from x_0. Thus, the subscript in the observing location relates to the progression of time as well.

During the final period of the MURI project, we have worked on reducing the computational complexity of the new approach and collaborated rather closely with the Texas A&M team to interface the new visibility algorithm with their point cloud learning code as well as testing the integrated code in the USC MOUT simulation site; in the MURI Final Review, we had demonstrated a satisfactory performance of the integrated code in autonomous and full 3D exploration using the simulated MOUT site.

In addition, during this last period of the MURI project, we started to analyze the performance of the new visibility algorithm – to obtain some fundamental understanding on how many vantage points, with respect to the geometrical and topological complexity of the obstacles in the scene, will be generated by the new algorithm in order to obtain complete visual surveillance of the scene (i.e. no blind spots), and if there were a known ***optimal*** algorithm, how does the current solution compare with the optimal solution? In Figure 35, we show the vantage point locations as planned by our algorithm for complete surveillance of two and four spheres in a scene. Our many

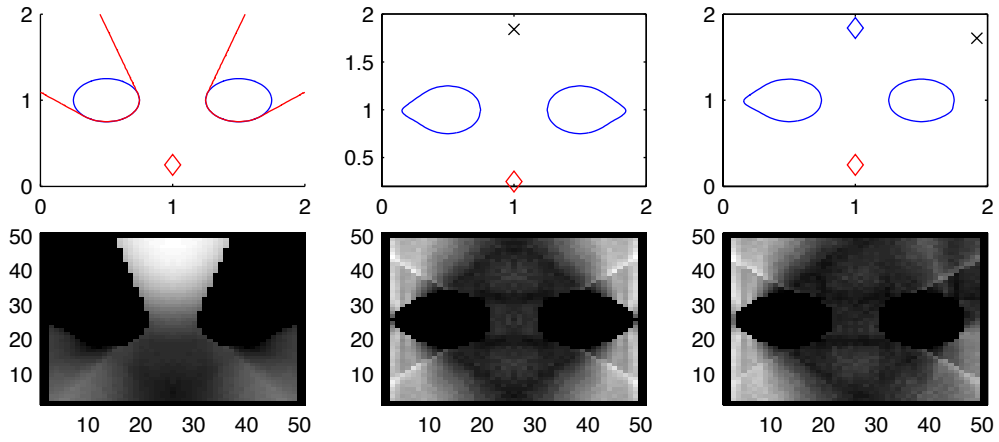

FIGURE 32. Generation of an "optimized" set of observing locations via the use of a visibility metric μ defined in (12). The blue curves shown in the top row are the estimates of the obstacles obtained from the observing locations. The crosses correspond to the newly added observing location. The diamonds indicate the observing locations. The images on the second row show the values of the visibility metric so that the whiter the color at a point, the larger the value is.

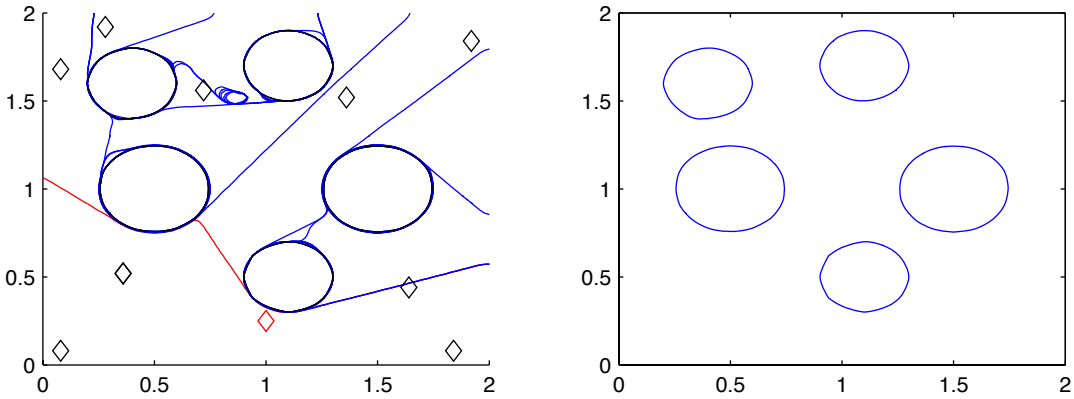

FIGURE 33. A simulation involving online-visibility estimates for mapping out the obstacles in the domain. The plot on the left shows the constructed observing locations in diamond shape and the obstacle estimates as well as the shadow boundaries at different stages. The plot on the right shows the estimated obstacles.

experiments suggest that with each additional sphere in the scene, only 1 or 2 additional vantage points are required, and this type of performance seems to be stable with respect to perturbation in the sphere sizes and spatial arrangements. In Figures 36 and 37 we show similar efficiency in vantage point placement for more complicated pipeline (topological) configurations.

This particular line of research was a new initiative of our MURI project and the strong potential which was exposed, has enabled the further development of this research through additional ARO support.

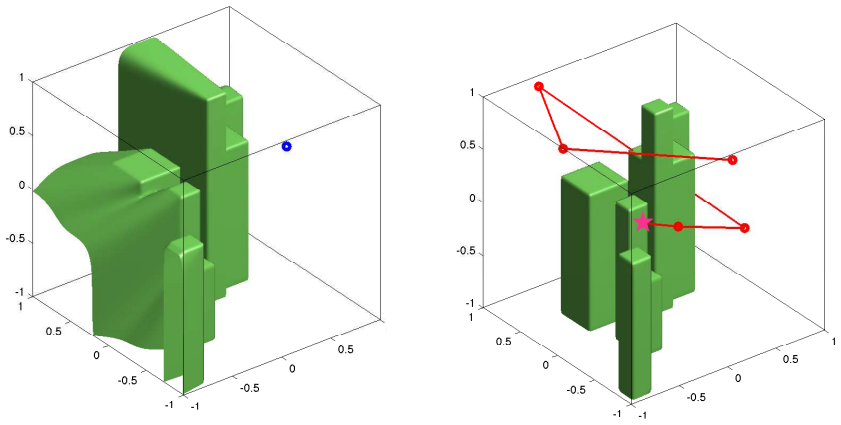

FIGURE 34. A simulation using the new visibility metric based algorithm in a 3D domain. Note that the green surfaces are the intersections of all the shadow boundaries, and when complete visibility of the free space is obtained by the vantage points, the green surface will correspond to the obstacles' surface.

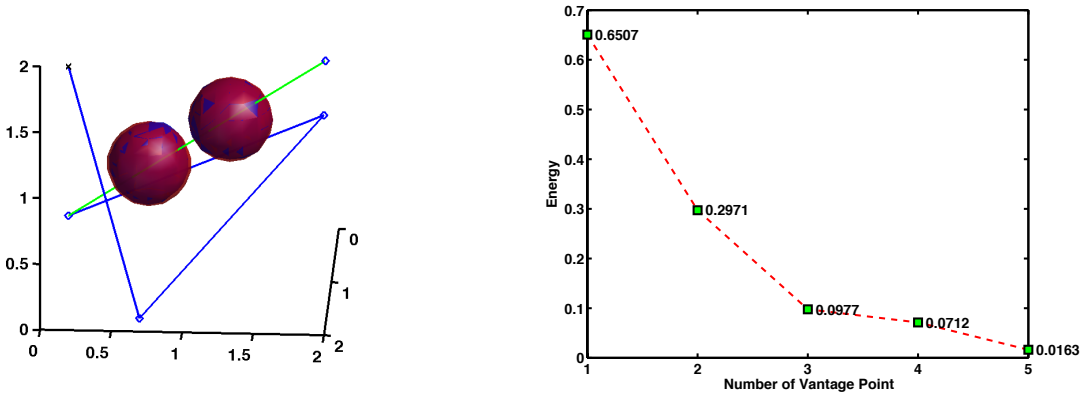

FIGURE 35. The performance of the new visibility algorithm for exploring two and four spheres. The left plot shows the decay of the ***energy*** additional vantage points are being added. Notice that the number of vantage points needed seem to grow linearly with the number of spheres in the scene.

6. VERIFICATION AND DATA ACQUISITION

The development and testing of algorithms and software for terrain rendering is very dependent on having robust data sets. Unfortunately, the project has been unable to obtain sufficient satisfactory data sets which can be used demonstration of our algorithm advances. In order to address this deficiency, the project has taken two steps: (i) develop simulators for realistic LIDAR data generation, (ii) generate the project's own data sets and test its software at available test sites.

6.1. **Enhanced *USC Simulator* Capability.** Building upon a previous collaboration with VT project personnel, USC enhanced the capability of its simulator of a virtual environment of the Ft. Benning MOUT site. The earlier version was designed to generate flight video which was used

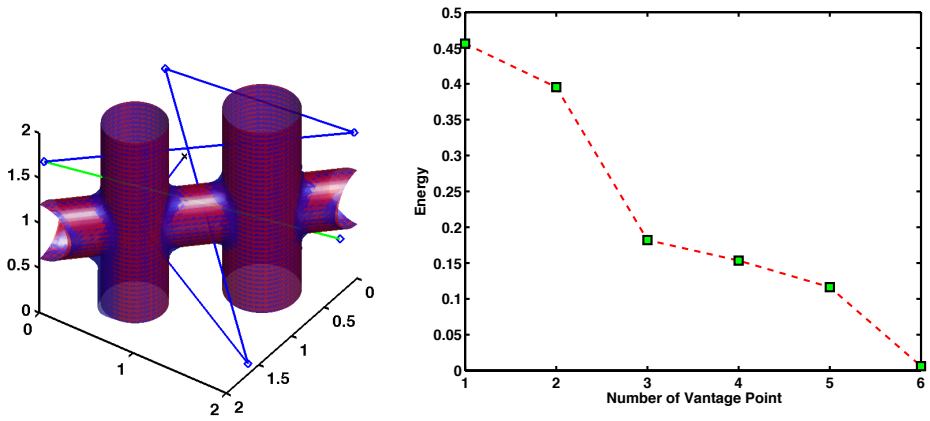

FIGURE 36. The performance of the new visibility algorithm for exploring a simple 3D pipeline configuration. The right plot shows the decay of the ***energy*** additional vantage points are being added.

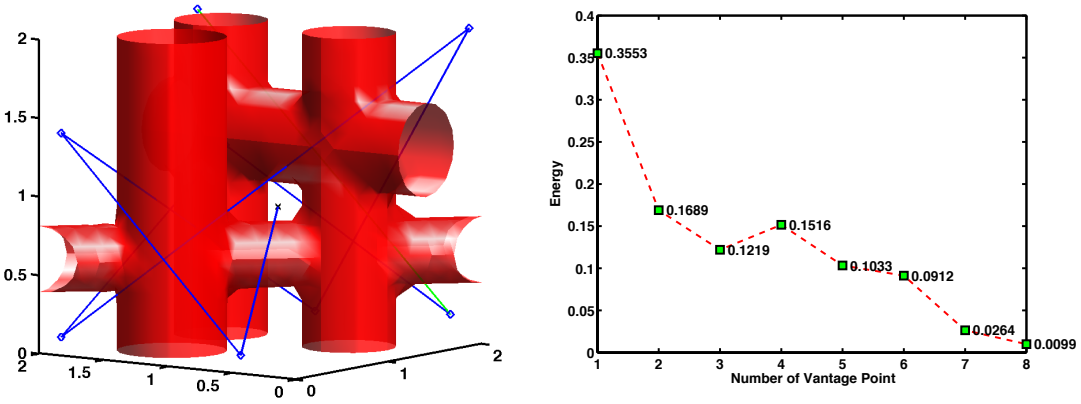

FIGURE 37. The performance of the new visibility algorithm for exploring a slightly more complex 3D pipeline configuration. The right plot shows the decay of the ***energy*** additional vantage points are being added. Notice that the number of vantage points needed seem to grow linearly with the number of spheres in the scene. Notice also in the left subfigure the symmetry of the planned vantage point locations.

to develop autonomous navigation algorithms using vision-based Structure From Motion (SFM) point clouds. In years one through three of the project the capabilities of the simulator were upgraded and enhanced to include additional sensor models and capabilities, including lidar. These improvements also included an improved interface that allowed for direct control of the simulator via Matlab as well as remote control over a local area network. The simulator allows the virtual deployment of multiple mobile platforms (ground and airborne) to generate sensor data within the virtual environment. The textured geometric data base originally used Open-Flight data structures and has been extended to incorporate several more popular 3D and texture formats. The added support of additional formats allows for existing assets typically created for high-end games to be retasked for the ARL-suggested surveillance and change-detection experiments among other simulated exercises. See Figure 38.

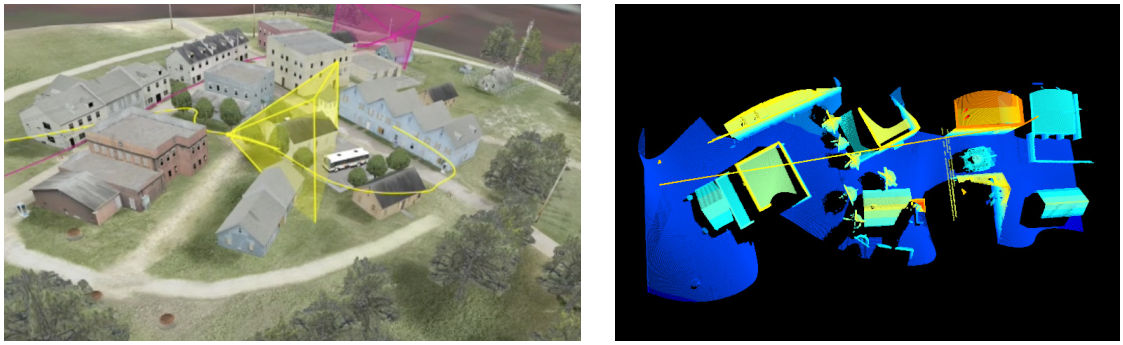

a) b)

FIGURE 38. Project Simulation capabilities: a) Multiple vehicle sensor packages (purple frustrum for ground vehicle, yellow for air) moving along designated paths, b) lidar simulated point cloud acquired along flight path (colored by height).

In years four and five the capabilities of the simulator were extended with various model sensors, including SICK, PILAR and Flash Lidar, which may be tested for real-time analysis of generated point clouds, design of sensor packages, and testing of collaborative dynamic sensor positioning. Additionally, external packages were updated to augment the simulator for applications such as feature tracking, SFM and point cloud editing. The in-house rendering engine used by the simulator was also updated to use the acceleration structures found in OpenSceneGraph. This update reduced rendering times and allowed for both lidar and camera sensors to share data structures used during simulated data acquisition.

In order to further develop one of the project's designated demonstration application areas, the simulator has been coupled with MAV flight control modules created using Simulink and Matlab in order to design and test autonomous navigation algorithms using MURI surfaces constructed from vision and lidar sensors. Moreover, the simulator has been designed to easily accommodate and visualize line-of-sight algorithms for MURI constructed surfaces.

As part of a collaboration with TAMU, an effort began late in year five to replace the in-house engine with Unity, a cross-platform and well supported game engine. The inclusion of the new engine will allow simulated scenes to contain higher polygon counts and thus provide more realistic simulated sensor data. Along with this update to the software, efforts are underway to update and improve the realism of the individual assets, including more realistic and higher-polygon flora.

6.2. **Experimental Verification.** The MURI team places a high value on experimental verification and validation of the theory, algorithms and software developed in this research program. Experimental field testing of the research in this MURI program prepares the team in providing direct, pertinent research to DoD laboratories. It should be emphasized that the MURI has supported the researchers and their assistants in their development of parts of the testbed, but the hardware components of the testbed itself are assets of the Unmanned System Laboratory at Virginia Tech. Virginia Tech has extended its techniques for creating dynamic point cloud measurement from experiment to include point cloud data from two rotationally articulating LIDAR line scanners. One drawback of the previous configuration described in the last report was that LIDAR data collection was restricted to fixed orientation with respect to the experimental vehicle. This meant that data acquisition was limited to only certain directions relative to the vehicle trajectory for one experiment.

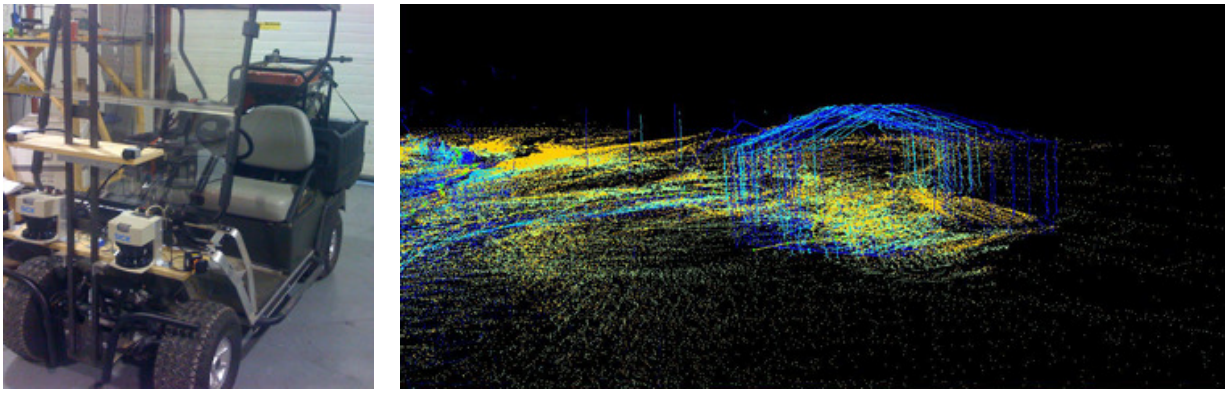

a) b)

FIGURE 39. a) Year 1 Virginia Tech ground vehicle equipped with a six sensor package which includes 2 horizontal line-scanning lidar, 2 vertical line-scanning lidar, stereo video, and an integrated IMU/GPS unit, b) Four channels of raw lidar data, colored-tagged by the appropriate lidar sensor, and coregistered.

A great deal of time and effort was required to construct the vehicle trajectory that would have sufficient point cloud density. The Virginia Tech testbed now can provide dynamically collected data sets to the MURI team members of a much higher density, which was a significant drawback to the earlier efforts. Now the Unmanned Systems Laboratory at VTech is capable of collecting dynamic data sets from a system that is configurable with a subset of (1) two stereo vision cameras operating at a maximum resolution of 640x480 at 60hz frame rate, (2) two channels of 80 meter range, single-line-scan LIDAR units, (3) two channels of 30 meter range single-linescan, (4) two articulating rotating LIDAR units, and/or an (4) IMU/GPS. South Carolina researchers have continued to work in a support role to the VTech team's data collection efforts by (i) collaborating in the design and coding of the Application Programmers Interfaces (API) for hardware and software integration of real-time data assimilation from the sensors, (ii) providing a real-time on-board 3D renderer of the scene for initial testing.

7. TECHNOLOGY TRANSFER: TRANSITIONING AND OUTREACH

The success of this project will be measured by the usefulness of the technology that it develops. This is dependent on the project having significant recognition in the defense community and having specific transitioning projects.

7.1. **Transitioning.** The project has made significant efforts for transitioning its technology to the defense sector. Through a number of transition/evaluation opportunities identified by the ARO Program, project members have interacted with researchers from ARL-Adelphi, AFRL-WP, defense industry contractors, and NATO SET-118 appointed members in order to gain insight into relevant DOD problems, current methods of approach, and the obstacles to meeting defense needs. This effort helped guide the project's formulation of application areas and challenge problems.

7.1.1. *Formal Industrial Collaborations: SBIR/STTR projects.* Project members were directly involved in technology transfer through funded Phase II SBIR and STTR awards. South Carolina personnel (Sharpley, DeVore, Hielsberg and Binev) teamed with Radiance Technologies (Andrew Thies, PI) as its industrial partner to provide geometric mapping and navigation capabilities to the

war fighter in an ARO-STTR entitled “Software for Generating Geometrically and Topologically Accurate Urban Terrain Models Using Implicit Methods”. Further, Radiance (Thies, PI) teamed with South Carolina (Sharpley) and Virginia Tech (Kurdila) to work on an AFRL-funded SBIR Phase II project entitled “Innovative Micro Air Vehicles & Control Techniques for Urban Environments”. The objective of the project was to provide surveillance, mapping, autonomous navigation and control capabilities for micro-aerial vehicles in real-time. These projects were successfully completed in March 2010 and November 2011, respectively.

7.1.2. *Sponsored International Defense Collaboration: NATO Research Task Group SET-118.* A MURI project member (Sharpley) was appointed to a three year term as a US representative to the NATO Research and Technology Organization (RTO) Research Task Group (RTG) on Ò3D-Modelling of Urban TerrainÓ (SET-118). Briefly, this task group was formed to study various representation forms for objects in urban terrain, to inspect procedures for automatic scene reconstructions by exploiting the data of modern sensors, and to discuss potential assessment metrics and criteria, as well as interoperability in terrain databases. The sensor technologies investigated covered active and passive sensors, such as flash laser, video, and interferometric SAR. A fuller discussion of the relevance of 3D models and military applications which benefit from the existence of 3D information, were itemized and discussed in its final report [15].

7.1.3. *Army Research Lab Collaboration: ARL Adelphi.* A student at UCLA, Zhaohui Guo, visited the ARL Adelphi Lab for 3 weeks and worked with Nasser Nasrabadi’s group on Change Detection and Surveillance, in particular on DR/FR/Mines data sets. He introduced fused lasso together with L_1 template matching. This improved existing hyperspectral target detection algorithms. The investigators have also considered combining this with dictionary based approaches. A prior rank, intensity, and sparsity models, based on robust PCA and tight frame regularization methods has also been developed. It has been applied very successfully to track objects in a noisy video at the ARL Adelphi Laboratory parking lot.

Figure 23 shows a single frame of a video surveillance stream from a parking lot at the Adelphi Army base. The upper left shows the scene with 40% randomly chosen missing points. The upper right figure depicts the difference between two successive frames. The lower left frame is the result of application of the robust PCA algorithm of [14]. This method uses L_1 theory to find the sparse component (background) and the nuclear norm to find the low rank component (motion). Our method, devised in [29] uses the tight frame decomposition of [13], minimizing the L_1 sum of the coefficients. These results are extremely promising and suggest new avenues for achieving state-of-the-art surveillance. One potential and promising approach is the possibility of combining the methodology with the fast interpolation of point clouds of [28] to do point cloud separation, (including motion) into a low rank and sparse decompositions.

7.2. **Data Security and Control.** Raw data sets, manuscripts and formal powerpoint presentations were provided by NATO SET-118 member organizations to the South Carolina component of the MURI for use in Urban Terrain Research. These research materials were provided under a FOUO classification (“For Official Use Only”) and under the agreement that SET-118 data collections would be accessed only by NATO citizens, unless permitted explicitly in writing by the NATO partner providing a data collection. The South Carolina component has complied with this agreement and has safely secured all materials. Four individuals from South Carolina have had access to this data (R. Sharpley, M. Hielsberg, S. Johnson, and J. Winders) and each has signed a technology control form specifically written for this project. The Form (see attachment **Be sure to !insert!**) states that the person who is granted access to the data acknowledges that technology

restrictions apply to non-NATO citizens, and the requirement to formally document and track any transfer of sensitive technology. The signed technology control forms have been kept in a secured IMI Firebox, along with original storage media containing the NATO materials which were provided by the NATO SET-118 leadership. Digital copies of SET-118 materials are also kept on a secure server to which only the four individuals had secure login access. The server is able to be accessed only through a secure local gigabit network. The firebox was kept in a locked file cabinet (in the IMI laboratory), to which only M. Hielsberg and R. Sharpley had keys. Laboratory doors were locked at all times.

7.3. **Project Management and Outreach.** The South Carolina team was responsible for the overall organization and coordination of the project during the first three years of the project. Management during the out-year extension (Years 4-5) passed to the Virginia Tech team.

A website (http://imi.cas.sc.edu/MURIwebsite) is maintained to facilitate collaboration and to promote the MURI findings and activities. In addition to describing on-going activities, the website provides Data and Code repositories available to project members via secure logins. In particular the *USC simulator* has been made available to all the MURI participants. The data which has been developed and collected is used to test algorithms and includes both simulated and real point clouds derived from vision, lidar and other sensors.

REFERENCES

[1] M. Belkin and P. Niyogi, *Laplacian eigenmaps for dimensionality reduction and data representation*, Neural Comput., 15(2002), pp. 1373-1396.

[2] M. Belkin, J. Sun and Y. Wang, *Constructing Laplace operator from point clouds in* $\mathbb{R}^d$, Proceedings of the Twentieth Annual ACM-SIAM Symposium on Discrete Algorithms, New York, New York, 2009, pp 1031-1040.

[3] A. Belochitski, P. Binev, R. DeVore, M. Fox-Rabinovitz, V. Krasnopolski, and P. Lamby, *Tree Approximation of the Long Wave Radiation Parameterization in the NCAR CAM Global Climate Model*, Journal of Computation and Applied Mathematics, to appear.

[4] B. Berkels, P. Binev, D. A. Blom, W. Dahmen, R. Sharpley, and T. Vogt, *Optimized Imaging Using Non-Rigid Registration*, preprint, Jan. 2013.

[5] P. Binev, A. Cohen, W. Dahmen, and R. DeVore, *Classification using Reliable Sets*, preprint.

[6] P. Binev, A. Cohen, W. Dahmen, and R. DeVore, *Classification Algorithms using Adaptive Partitioning*, IMI Preprint Series 2012:07, University of South Carolina, 31 pp.

[7] P. Binev, A. Cohen, W. Dahmen, and R. DeVore, "Universal Algorithms for Learning Theory Part II: Piecewise Polynomials", *Constructive Approximation* **26.2** (2007), 127–152.

[8] Binev P., A. Cohen, W. Dahmen, R. DeVore, V. Temlyakov, "Universal algorithms for learning theory - Part I: piecewise constant functions", *Journal of Machine Learning Research* **6** (2005), 1297–1321.

[9] P. Binev, W. Dahmen, and P. Lamby, *Fast High Dimensional Approximation with Sparse Occupancy Trees*, preprint, on-line as IMI Technical Reports 10:03, 2010.

[10] P. Binev, W. Dahmen, and P. Lamby, "Fast high-dimensional approximation with sparse occupancy trees", *Journal of Computational and Applied Mathematics*, **235**(2011), 2063?2076.

[11] P. Binev and R. DeVore, "Fast Computation in Adaptive Tree Approximation", *Numerische Mathematik* **97** (2004), 193–217.

[12] A. M. Bronstein, M. M. Bronstein, R. Kimmel, M. Mahmoudi and G. Sapiro, *A gromov-hausdorff framework with diffusion geometry for topologically-robust non-rigid shape matching*, Int. J. Comput. Vis., 89(2010), pp. 266-286.

[13] J.-F. Cai, B. Dong, S. Osher and Z. Shen, *Image restoration: total variation, wavelet frames and beyond*, UCLA CAM Report 11-22, 2011.

[14] E. J. Candes, X. Li, Y. Ma and J. Wright, *Robust principal component analysis*, Tech Report, Stanford University, 2009.

[15] D. Carrasco Diaz (ESP), J. Fournier (CAN), J. Lavery (USA), R. Sharpley (USA), K. McEwan (GBR),J. Meidow (DEU), S. Pasquariello (ITA) and G. Tolt (SWE), *3D Modeling of Urban Terrain*, NATO Research and Technology Organization Task Group, RTO-TR-SET-118, Sept 2011, pp 118. [ISBN: 978-92-837-0144-6]

[16] E. Castillo, J. Liang, and H. Zhao *Point cloud segmentation and denoising via constrained least squares normal estimates* Book Chapter, Innovations for Shape Analysis: Models and Algorithms, Springer, 2012.

[17] T.-F. Chan and L.-A. Vese, *Active Contours without Edges*, IEEE Transactions on Image Processing, v.10, pp.266-277, 2001.

[18] T.M. Chan, *Semi-Online Maintenance of Geometric Optima and Measures*, *SIAM J. Comp*, Vol 23, 700-716, 2003.

[19] U. Clarenz, M. Droske and M. Rumpf, *Towards fast non–rigid registration*. In "Inverse Problems, Image Analysis and Medical Imaging", AMS Special Session Interaction of Inverse Problems and Image Analysis, Vol 312, pp 67–84, Amer. Math. Soc., 2002.

[20] R. R. Coifman and S. Lafon, *Diffusion maps*, Appl. Comput. Harmon. Anal., **21**(2006), pp. 5-30.

[21] V. Chandrasekaran, M.B. Wakin, D. Baron, and R.G. Baraniuk, *Representation and Compression of Multidimensional Piecewise Functions Using Surflets,* IEEE Transactions on Information Theory, Vol. 55, No. 1, January, 2009, pp. 375-400.

[22] A. Cohen, I. Daubechies, R. DeVore, G. Kerkyacharian and D. Picard, *Capturing Ridge Functions in High Dimensions from Point Queries* , Constructive Approximation, to appear.

[23] Z. Deng, J. Gregory and A. Kurdila, Learning Theory with Consensus in Reproducing Hilbert Spaces, *Submitted to the 2012 IEEE American Control Conference*, June, 2012.

[24] Z. Deng, J. Gregory and A. Kurdila, Convergence Rates for Learning Theory with Consensus, *Submitted to the 2012 IEEE Conference on Decision and Control*, December 2012.

[25] R. DeVore, G. Kerkyacharian, D. Picard and V. Temlyakov, *Mathematical Methods of Supervised Learning*, Technical report 0422, IMI, University of South Carolina, Columbia, 2004.

[26] R. DeVore, G. Petrova, M. Hielsberg, L. Owens, B. Clack, and A. Sood, *Processing Terrain Point Cloud Data*, SIAM Journal on Imaging Sciences, **6** (2013), pp. 1-31.

[27] R. DeVore, G. Petrova, and P. Wojtaszczyk, *Approximating Functions of Few Variables in High Dimensions* Constructive Approximation, **33**(2011),125-143.

[28] V. Estellers, D. Zosso, R. Lai, J.-P. Thiran, S. Osher and X. Bresson, *An efficient algorithm for level set method preserving distance function*, preprint, 2011.

[29] H. Gao, H. Yu, S. Osher and Ge Wang, *Multi-energy CT based on (PRISM*, UCLA CAM Report 11-01, 2011.

[30] T. Goldstein, X. Bresson and S. Osher, *Geometric applications of the split Bregman method*, *J. Sci. Comput.* v.45, (2009), pp. 272-293.

[31] T. Goldstein and S. Osher, *The split Bregman method for L1 regularized problems*, *SIAM J. Image Sci.*, v.2, (2009), pp. 323-343.

[32] D. Jimenez, G. Petrova, *On Matching Point Configurations*, submitted.

[33] B. Karaivanov, *A self-adjusting region growing algorithm for geometric segmentation*, in preparation.

[34] A. Kurdila, M. Nechyba, R. Lind, P. Ifju, P. Binev, W. Dahmen, R. DeVore, and R. Sharpley, "Vision-Based Control of Micro-Air-Vehicles: Progress and Problems in Estimation", *43rd IEEE Conference on Decision and Control*, Paradise Island, Bahamas, (December 2004), 1636–1642. Appeared IEEE Decision and Control.

[35] R. Lai, J. Liang and H. Zhao, *A local mesh method for solving partial differential equations on point clouds*, SIAM Journal on Scientific Computing, (to appear).

[36] R. Lai and S. Osher, *A splitting method for orthogonality constrained problems*, UCLA CAM Report 12-39, (2012)

[37] R. Lai, Y. Shi, K. Scheibel, S. Fears, R. Woods, A. W. Toga and T. F. Chan, *Metric-induced optimal embedding for intrinsic 3D shape analysis*, IEEE Conference on Computer Vision and Pattern Recognition (CVPR), 2010.

[38] Y. Landa. *Visibility of point clouds and exploratory path planning in unknown environments*. PhD thesis, UCLA, 2008.

[39] Y. Landa and R. Tsai. Visibility of point clouds and exploratory path planning in unknown environments. *Comm. Math. Sci.*, 6(4):881–913, 2008.

[40] B. Levy, *Laplace-Beltrami eigenfunctions towards an algorithm that "understands" geometry*, IEEE Conference on Shape Modeling and Applications, 2006.

[41] R. Lai, J. Liang, A. Wong, and H. Zhao *Geometric Understanding of Point Clouds Using Laplace-Beltrami Operator*, IEEE Conference on Computer Vision and Pattern Recognition (CVPR), 2012.

[42] J. Liang, F. Park and H. Zhao *Robust and efficient implicit surface reconstruction of point clouds based on convexified image segmentation* Journal of Scientific Computing, to appear.

[43] J. Liang and H. Zhao, *Solving partial differential equations on point clouds*, SIAM Journal on Scientific Computing, under revision.

[44] J. Manson, G. Petrova, S. Schaefer, *Streaming surface reconstruction using wavelets*, Computer Graphics Forum (Proceedings of the Symposium on Geometry Processing), **27** (2008), no. 5, 1411–1420.

[45] X. Bresson, S. Esedoglu, P. Vandergheynst, J. Thiran, and S. Osher, *Fast Global Minimization of the Active Contour/Snake Model*, Journal of Mathematical Imaging and Vision, v.28, pp.151-167, 2007.

[46] Kazhdan, M., Bolitho, M., and Hoppe, H., *Poisson Surface Reconstruction*, Eurographics Symposium on Geom. Process., 2006, 61–70.

[47] F. Preparata and M. Shamos, *Computational Geometry: An Introduction*, Springer, 1985.

[48] D. Raviv, A . M. Bronstein, M. M. Bronstein, R. Kimmel and N. Sochen, *Affine-invariant diffusion geometry for the analysis of deformable 3D shapes*, IEEE Conference on Computer Vision and Pattern Recognition (CVPR), 2011.

[49] C. Scott and R. Nowak, *Minimax-optimal classification with dyadic decision trees*, IEEE Transactions on Information Theory **52**(2006), 1335Ð-1353.

[50] J. Smith, G. Petrova, S. Schaefer, *Progressive Encoding and Compression of Surfaces using Point Cloud Data*, preprint.

[51] J. Sun, M. Ovsjanjkov and L. Guibas, *A concise and provably informative multi-scale signature based on heat diffusion*, Proc. SGP, 2009.

[52] R. Takei and R. Tsai. Optimal trajectories of curvature constrained motion in the hamilton-jacobi formulation. *Under review*, 2008.

[53] R. Takei, R. Tsai, H. Shen, and Y. Landa. A practical path-planning algorithm for a vehicle with a constrained turning radius: a Hamilton-Jacobi approach. In *ACC*, 2010.

[54] A. Waters and R.G. Baraniuk, *Multiscale Point Cloud Representation and Compression using Hausdorff Distortion*, Preprint, 2012.